

Highlights

Heliostat-field soiling predictions and cleaning resource optimization for solar tower plants

Cody B. Anderson, Giovanni Picotti, Michael E. Cholette, Bruce Leslie, Theodore A. Steinberg, Giampaolo Manzolini

- Cleaning resources evaluated in the design phase of a modular solar tower power plant.
- Soiling prediction methodology allows multiple soiling trajectories to be evaluated.
- Parking heliostats horizontally at night reduces plant productivity.
- CSP night-time power generation dispatch policies can tolerate higher soiling loads.
- Cleaning during day reduces production for a negligible reflectance based production gain.

Heliostat-field soiling predictions and cleaning resource optimization for solar tower plants

Cody B. Anderson^{a,b,*}, Giovanni Picotti^a, Michael E. Cholette^a, Bruce Leslie^c, Theodore A. Steinberg^a, Giampaolo Manzolini^b

^a*School of Mechanical, Medical and Process Engineering, Queensland University of Technology, 2 George Street, Brisbane, 4000, QLD, Australia*


^b*Dipartimento di Energia, Politecnico di Milano, Via Lambruschini, 4, Milano, 20156, Lombardy, Italy*

^c*Vast, 225 Brisbane Terrace, Ipswich, 4300, QLD, Australia*

Abstract

One of the primary cost drivers for concentrated solar power operations and maintenance is the soiling of heliostats in the solar field. Although this loss can be largely recovered through cleaning operations, the associated costs are substantial and require careful consideration in relation to productivity gains.

This paper presents a novel methodology for characterizing soiling losses through experimental measurements. Soiling predictions were obtained by calibrating a soiling model based on field measurements from a 50 MW modular solar tower project in Mount Isa, Australia. The study found that the mean predicted soiling rate for horizontally fixed mirrors was 0.12 pp/d during low dust seasons and 0.22 pp/d during high seasons. Autoregressive time series models were employed to extend two years of onsite meteorological measurements to a 10-year period, enabling the prediction of heliostat-field soiling rates. A fixed-frequency cleaning heuristic was applied to optimise the cleaning resources for various operational policies by balancing direct cleaning resource costs against the expected lost production, which was computed by averaging multiple simulated soiling loss trajectories. Analysis of resource usage showed that the cost of fuel and operator salaries contributed 42% and 35% respectively towards the cleaning cost. In addition, stow-

*Corresponding author Cody B. Anderson 
Email address: cb.anderson@qut.edu.au (Cody B. Anderson)

ing heliostats in the horizontal position at night increased daily soiling rates by 114% and the total cleaning costs by 51% relative to vertically stowed heliostat-field. Under a simplified night-time-only power production configuration, the oversized solar field effectively charged the thermal storage during the day, despite reduced mirror reflectance due to soiling. These findings suggest that the plant can maintain efficient operation even with a reduced cleaning rate. Finally, it was observed that performing cleaning operations during the day led to a 7% increase in the total cleaning cost compared to a night-time cleaning policy. This was primarily attributed to the need to park operational heliostats for cleaning.

Keywords: CSP, Heliostat, Soiling, Reflectance, Forecast, Cleaning resources, Operation and maintenance

1. Introduction

The transition towards renewable energy is underway globally to mitigate the effects of climate change. Throughout 2019, Oceania was the fastest growing region in the world with an 18.4% renewable capacity increase to 40 GW [1]. Australia has the highest average solar radiation per square metre of any continent in the world [2]. This potential has thus far been exploited via PV. However, CSP remains a promising technology owing to the economic advantages of its use with TES, which is competitive with similarly-sized PV installations with electrochemical storage [3].

One of the key challenges for CSP is the O&M costs, which can be significantly higher than competing technologies [4]. A unique cost driver is the accumulation of soil on heliostats, which can quickly diminish the field specular reflectance and thus the productivity of the plant [5–10]. Changes in reflectance with time (i.e. soiling rate) can vary widely in time and between sites. For example, Hachicha et al. [11] report a soiling rate of 2.13 percentage points per day (pp/d) in the United Arab Emirates, and Azouzoute et al. [12] reported losses of 0.35 pp/d for a 25° fix tilt mirror in Morocco. A long term Madrid soiling campaign by Conceição et al. [13] measured soiling rates between 0.13 pp/d to 0.58 pp/d depending upon the season and long-range transports of Saharan desert dust. Moreover, the key factors influencing this variation (location, field and plant design, seasonality, etc.) are not well understood. This poor understanding of soiling rates increases productivity revenue uncertainty and operational costs. This is particularly problematic

during plant design. A better understanding of site soiling characteristics early in the plant design would enable more informed decisions on cleaning policy, site suitability, and possible design modifications (e.g. over-sizing the field) [10].

Predictive models for soiling rates have been the subject of a large number of studies in both the PV and CSP literature. These models can be separated into two broad classes: regression/empirical models (e.g. ANN, ARMA, linear regression) [14–16] and physical models, which are usually based on atmospheric deposition models [17–19].

In one study by El Boujdaini et al. [20] trained an ANN to predict soiling losses of a TraCs [21] soiling station in Eastern Morocco over a 20 week period. Alternatively, Ballestrín et al. [22] predicted soiling losses of a PV system by training an ARMA model using 8 months of electrical loss measurements due to soiling. The fitted ARMA model was then able to predict 38 days of soiling losses with a mean relative error of 3.12% between predictions and actual measurements. The main drawbacks to these empirical models are their lack of physical interpretations of the parameters, poor portability to different sites, and the need for large amounts of data for reliable predictions.

Other studies, have pursued physical models as Picotti et al. [17] who developed a physical DSM and validated for a fixed tilt angle solar mirror. The model utilises meteorological measurements and the solar field design to predict the particle deposition velocity and eventually soiling rates with a relative error of 14% between the model and measurements. Similarly, Sengupta et al. [19] adapted a particle deposition velocity and wind removal model to predict the transmittance and the dust deposition density of an outdoor PV module over 15 days. The deviation between measured and predicted dust deposition density was found to be 4.84%. A weakness in these studies is the specular reflectance loss model — which is either not needed (i.e. for PV studies) or was based on a first-surface reflector (while most CSP mirrors are second-surface).

Once the site soiling is understood, some researchers have aimed to optimize cleaning strategies for fixed field designs. For instance, Picotti et al. [23] conducted a study comparing two time-based cleaning optimization strategies based on daily soiling rate predictions obtained from a physical soiling model [17]. The results demonstrated that simple heuristic approaches performed as effectively as more complex and theoretically optimal planning methodologies. Specifically, the simple heuristic achieved near-optimal performance, with only a marginal deviation, while requiring significantly lower

computational costs.

Similarly, Wales et al. [24] explored a similar formulation, considering a fixed monthly soiling rate for the solar field to optimize the allocation of permanent and seasonal cleaning workers over a ten-year period.

Alternatively, reflectance-based policies have been applied to the optimization of heliostat cleaning [25, 26] whereby the decision to clean is triggered when a heliostat’s reflectance falls below a threshold value. Truong-Ba et al. [27] utilised a sectorial condition-based cleaning policy to optimize cleaning resources for a hypothetical CSP plant over a ten-year horizon. While all policies resulted in the same number of cleaning crews being deployed, the sectorial condition policy exhibited a cost-saving of 2.08% relative to a time-based cleaning policy.

Although some research has explored loss models and cleaning optimization, there remains a gap in the literature regarding reflectance loss in Australian locations relevant to CSP. Consequently, typical loss rates specific to these regions are not yet established. Furthermore, existing studies on cleaning optimization often assume the availability of long-term soiling loss models (e.g., loss dynamics over several months), either by treating them as constant [24] or by calibrating physical models for future plant/sites. While it is clear that the constant models have serious limitations, it is not yet clear how to develop long-term loss models from limited site data — particularly when historical data from weather stations is not sufficiently close to the site (a likely case for the remote locations typically considered CSP candidate sites). Lastly, current cleaning approaches are not adequately tailored for soiling planning during the design phase.

This study details a new methodology used to characterize soiling losses through experimental measurements and predict ongoing soiling losses using an extended DSM [17] for a 50 MW modular solar tower site in Australia. The previously developed DSM is extended to include a second-surface loss model to better represent the mirrors that are to be used in the future plant. An experimental procedure for collecting soiling-related data for a candidate site is detailed, and data analysis techniques are developed to characterize the airborne dust and other meteorological parameters to predict particle deposition rates and their statistical variability. Cleaning resources for the future plant are optimized using a stochastic extension adapted from Picotti et al. [23] minimizing the *average* total cleaning costs (sum of productivity losses and cleaning costs). The novelty of this study extends beyond the soiling characterization and optimization methodology. For the first time,

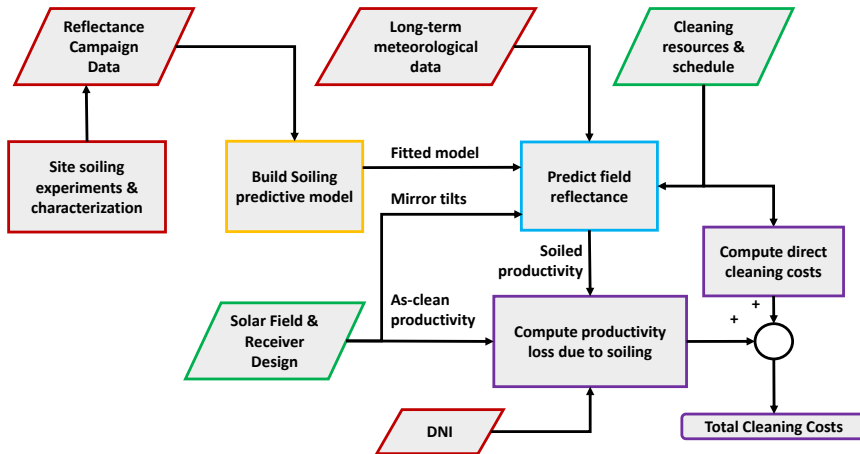


Figure 1: Overview of Cleaning Resource Optimisation Procedure

an assessment of cost implications related to operational choices is undertaken. This includes factors such as daytime cleaning, stowing positions, and constraints linked to the receiver and storage systems.

The remainder of the paper is organized as follows. Section 2 introduces the soiling model and cleaning resource heuristic. Section 3 presents the developed methodology as part of a case study to optimize the cleaning resource needs of a candidate CSP hybrid solar plant with conclusions drawn in section 4.

2. Methodology

An overview of the soiling prediction and cleaning optimization methodology is shown in Fig. 1. An optimal strategy will minimize the total cleaning cost that is calculated as the sum of the direct cleaning costs¹ and revenue losses due to soiling induced productivity loss. Solar field reflectance predictions are computed using a fixed cleaning schedule, corresponding to a number of deployed cleaning crews and cleaning frequency. During a cleaning event a reflectance recovery model is used to calculate the number of particles remaining depending upon the cleaning technology used. Solar field soiling rates are created using a site calibrated DSM for several simulation trajectories using ambient temperature, wind speed, and TSP. The DSM is tuned to

¹Direct cleaning costs include salaries, truck depreciation, fuel, and water

the CSP site through a site soiling experimental and characterization, where local soiling properties have been experimentally determined. The proposed methodology detailed below allows for the optimisation of cleaning resources under stochastic soiling trajectories early within the site selection and CSP design stage of a power plant.

2.1. Soiling Predictive Model and Second Surface Geometry Factor

The cumulative number of particles deposited onto the surface of a heliostat is computed as

$$N_k(D) = \sum_{i=1}^k n_i(D) \cdot \Delta t \quad (1)$$

where D is the particle diameter (assumed spherical), Δt is the sample period and $n_i(D)$ is the rate of deposition during the sample period, as determined from the DSM[4]. Typically, Δt is the sampling period of the meteorological measurements (wind speed, airborne dust, etc.) which is constant.

The cumulative number of particles adhered to a heliostat at time k is computed as an effective reflective area loss due to soiling with:

$$A_k^{\text{loss}}(\theta_k) = \int_0^{\infty} N_k(D) \cdot a(\theta_k, D) dD \quad (2)$$

Where $a(D)$, is the area lost to specular reflectance for a particle of diameter, D at incidence angle, θ . This factor depends both on the nature of the reflector and the density of the particles on the surface. Assuming that particles on the surface are well separated (i.e. do not block/shade the same area)

$$a(\theta, D) = A^{\text{shade}}(\theta, D) + A^{\text{block}}(\theta, D) - A^{\text{overlap}}(\theta, D) \quad (3)$$

The first two terms on the right-hand side are the shaded and blocked area of the reflector, which are elliptical with major axis $\frac{D}{\cos \theta}$ and minor axis D , so the area can be computed as

$$A^{\text{shade}}(\theta, D) = A^{\text{block}}(\theta, D) = \frac{\pi D^2}{4 \cos \theta} \quad (4)$$

The overlap area $A^{\text{overlap}}(\theta, D)$ is the area that is both blocked and shaded by a single particle. This is derived in Appendix A calculated analytically

as

$$A^{\text{overlap}}(\theta, D) = \frac{D^2}{2 \cos \theta} \cdot (\bar{t} - \sin \bar{t} \cdot \cos \bar{t}) \quad (5)$$

where \bar{t} is:

$$\bar{t} = \cos^{-1} \left(\frac{D - 2x_o \cos \theta}{D} \right) \quad (6)$$

Where x_o is the length of overlap of the blocking and shading ellipse (see Fig. A.21). This length can be computed (also in Appendix A):

$$x_o = \frac{D}{2} \tan \left(\frac{\pi}{4} - \frac{\theta}{2} \right) - t_g \tan \left(\sin^{-1} \left(\frac{n_{\text{air}}}{n_{\text{glass}}} \cdot \sin \theta \right) \right) \quad (7)$$

where n_{air} and n_{glass} are the refractive indices of air and glass, respectively, and t_g is the thickness of the glass between the particles and the reflective surface. Examining these equations, it is clear that $\theta \rightarrow 0$ yields an overlap

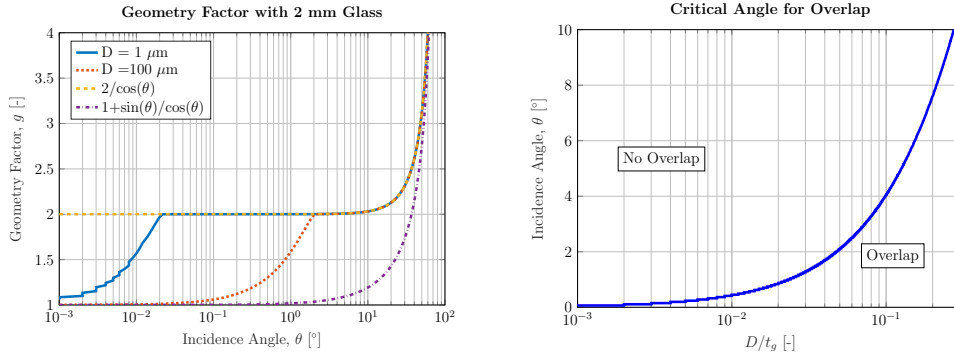


Figure 2: Left: Geometry factor for particle diameters and simplified first and second geometry models. Right: Incidence angles and particle size/glass thickness required for blocking and shading overlap.

area that is equal to the shading and blocking area, i.e. the area loss $a(\theta, D) = \frac{\pi D^2}{4}$ is simply equal to the cross-sectional area of the particle. In the other extreme, $\theta \rightarrow \frac{\pi}{2}$ yields no overlap. Thus, there is a critical incidence angle where overlap will occur that will be a function of D and t_g . This critical angle is shown in Fig. 2 right.

Figure 2 left compares a small and large particle's geometry factor which is calculated as

$$g = a(\theta, D) \cdot \frac{4}{\pi D^2} \quad (8)$$

i.e. it is the ratio of reflective area loss and the cross-sectional area of the particle. In the case of no overlap ($A^{\text{overlap}} = 0$), this yields

$$g = \frac{\pi D^2}{2 \cos \theta} \cdot \frac{4}{\pi D^2} = \frac{2}{\cos \theta} \quad (9)$$

This approximation is compared with the actual geometry factor and the first surface geometry factor in the left-hand side of Fig. 2 for $t_g = 2$ mm. The vast majority of airborne dust particles will typically be below 100 μm , so it can be said that the geometry factor approximation of (9) is valid for incidence angles above 1° , which encompasses the vast majority of incidence angles in a CSP tower plant [28]. This approximation yields the following expression for the area loss:

$$A_k^{\text{loss}}(\theta) = \frac{2}{\cos \theta} \cdot A_k^{\text{norm}}(D) \quad (10)$$

where

$$A_k^{\text{norm}} = \frac{\pi}{4} \int_0^\infty D^2 N_k(D) dD \quad (11)$$

is the total area loss with a normal incidence angle. Eventually, the reflectance is computed as

$$\hat{\rho}_k(\theta_k) = \rho_0 \left(1 - \frac{2}{\cos \theta_k} \cdot \frac{A_k^{\text{norm}}}{A^{\text{mirror}}} \right) \quad (12)$$

where A^{mirror} is the total mirror reflective area and ρ_0 is the as-clean reflectance.

2.1.1. Site Soiling Characterization

For accurate heliostat-field soiling predictions, the DSMs free parameter surface roughness ratio, h_r/z_o should be estimated from site data using solar mirror reflectance values measured on site [17]. Using the DSM, reflectance predictions throughout the measurement campaign may be made using the measured meteorological variables. A least mean squared fit between measured and predicted reflectance values may then be used to determine an

appropriate h_r/z_o as shown in (13):

$$h_r/z_o = \arg \min_h \sum_{k=1}^K (\rho_k - \hat{\rho}_k)^2 \quad (13a)$$

$$\text{s.t. } \hat{\rho}_{k+1} = f(\hat{\rho}_k, T_k, v_k, TSP_k, \phi_k; h) \quad (13b)$$

$$\hat{\rho}_0 = \rho_0(\text{measured}) \quad (13c)$$

where measured reflectance, ρ is measured during the experimental campaign and reflectance prediction, $\hat{\rho}$ is determined from the DSM and the relevant mirror properties and weather inputs in (13b) – the tilt angle, ϕ between horizon and solar mirror; wind speed, v , total suspended particles, TSP, and ambient temperature, T as measured from the weather station for each measurement, $k = 1, 2, \dots, K$.

In the absence of long term meteorological data, time series analysis can be used to extend existing meteorological data [29, 30] and explore several yearly trajectories. Since TSP data is non-normal (a key assumption for time series modelling) a common transform is employed:

$$y_k = \begin{cases} \log(TSP_k + \omega_k) & TSP > 0 \\ \log(TSP_k + \epsilon_k) & TSP = 0 \end{cases} \quad (14)$$

where TSP_k is the TSP measurement at time k , s is the resolution of the TSP measurements, $\omega_k \sim \mathcal{U}(0, \frac{\alpha}{2})$, and $\epsilon_k \sim \mathcal{U}(\frac{-s}{2}, \frac{\alpha}{2})$. This choice acknowledges that due to the resolution of the instrument, if a measurement has τ_k then the true value is in the range $[\tau_k - \frac{\alpha}{2}, \tau_k + \frac{\alpha}{2})$ if $\tau_k > 0$ and in the range $[0, \tau_k + \frac{\alpha}{2})$ if $\tau_k = 0$.

Using the transformed time series y_k , an autoregressive model of the form:

$$y_k = \sum_{i=1}^{n_a} \phi_i y_{k-i} + \kappa_k \quad (15)$$

is estimated from the data, where the noise terms κ_k are assumed to be normal, independent and identically distributed (i.i.d.) with variance σ_a^2 . The parameters are estimated via least squares for $n_a \in [1, 50]$ and the model with the minimal Akaike's Information Criterion is selected as the best model.

A similar approach was adopted for the wind speed. However, due to the diurnal non-stationarity of wind speeds, a Z-score normalization tech-

nique [31] was applied to standardize the data

$$u_k = \frac{v_k - \bar{v}_{\text{tod}(k)}}{\sigma_{\text{tod}(k)}} \quad (16)$$

where v_k is the nominal wind speed, and $\bar{v}_{\text{tod}(k)}$ and $\sigma_{\text{tod}(k)}$ are the average and standard deviation, respectively, of the wind speed during the same time of the day as k in the historical record (i.e. the wind speed statistics are assumed to be 24-hour-periodic).

2.2. Cleaning Resource Optimizer

Once h_r/z_o is estimated from the experimental site data, the DSM can be used to predict soiling rates for a hypothetical operating solar field using only meteorological data and solar field design conditions. The predicted soiling rates are utilised with a cleaning resource optimiser to determine a cost effective cleaning resource plan. Decisions of when to clean must consider the economic balance of cleaning costs and plant productivity. A FFTBCS policy was employed here, which has been shown to yield near-optimal cleaning schedules for the case where trucks are owned [23].

The FFTBCS policy is described as follows. Firstly, the field is sectorized into $j = 1, 2, \dots, J$ sectors, each of which has a representative heliostat for which the soiling losses are simulated by the DSM. All heliostats in the sector are assumed to have the same soiled area and incidence angle. There are M cleaning crews of which can each clean R sectors in one day of cleaning and the number of full-field cleans per year is $F \in 0, \text{floor} \frac{365 \cdot M \cdot R}{J}$. Since the sectors are cleaned in sequential order, the set of time indices where section $j = 1$ is cleaned is

$$\mathcal{D}_1 = \{1, \lceil \Delta k \rceil, \lceil 2\Delta k \rceil, \dots, \lceil (F - 1) \cdot \Delta k \rceil\} \quad (17)$$

where $\lceil \cdot \rceil$ denotes a rounding up operation and the number of days in between cleans, Δk is

$$\Delta k = \frac{365 \cdot \Delta t_d}{F} \quad (18)$$

where $\Delta t_d = \frac{24}{\Delta t}$ (Δt in hours) is the number of sampling periods in a day. The cleaning time for any sector $j = 2, 3, \dots, J$ are:

$$\mathcal{D}_j = \left\{ d + \text{floor} \left(\frac{j-1}{M \cdot R} \right) \mid d \in \mathcal{D}_1, j > 1 \right\} \quad (19)$$

The parameters of this model are (J, R, M, F) . The parameter J is selected based on the desired spatial resolution of the soiling predictions, while R is a function of the technology and number of people in a crew. Once these parameters are fixed, the FFTBCS policy is thus parameterized by M and F .

The optimal (M, F) are calculated by minimizing the total annual cleaning cost:

$$\text{TCC}(M, F) = C^{\text{cl}} + C^{\text{deg}} \quad (20)$$

where C^{cl} is an annualized sum of all direct cleaning related costs (i.e. fixed yearly costs and variable costs with number of field cleanings):

$$C^{\text{cl}}(M, F) = \left(\frac{C^{\text{truck}}}{b} + C^{\text{salary}} + C^{\text{maint}} \right) M + \sum_{j=1}^J C^{\text{w\&f}} \cdot A_j^{\text{total}} \cdot F \quad (21)$$

where C^{truck} is the cost of a cleaning vehicle, b is the useful life of the truck, C^{salary} is the cleaning vehicle operator salary, M is the number of cleaning crews, water and fuel costs, $C^{\text{w\&f}}$ represent the cleaning truck consumable costs per square metre of heliostat cleaned, and A_j^{total} is the heliostat area of sector j .

The degradation costs, C^{deg} are associated with the loss in thermal energy due to soiling and is calculated as the difference in revenue that would have been obtained from an always clean heliostat field and the predicted soiled reflectance values for the given cleaning schedule, as shown in (22).

$$C^{\text{deg}}(M, F) = (P - C^{\text{o\&m}}) \sum_{k=1}^K (w_k^{\text{clean}} - w_k^{\text{soil}}) \Delta t \quad (22)$$

where P is the sale price of electricity, $C^{\text{o\&m}}$ is the cost of non-cleaning operation and maintenance tasks per unit of power production², Δt is the time between two epochs (usually the sampling frequency of the meteorology data), w_k^{clean} and w_k^{soil} is the electrical work generated from a solar field in clean ($\hat{\rho} = \rho_0$) and predicted soiled conditions respectively at time k , and K is the total number of samplings for the simulation trajectory. The amount

²Thus, higher soiling losses lead to lower non-cleaning operation and maintenance costs, which is common in energy production economic analyses

of work produced for both the clean and soiled conditions depends on the plant design and operating strategy. The plant under consideration is one with thermal energy storage (no direct steam capability) and a number of receivers, each with their own dedicated solar field. A simplified dispatch strategy is adopted where the power block is run at rated load when the thermal storage is sufficient and shutdown otherwise.

When the energy from the storage is sufficient to run the power block at rated loads for the full duration (i.e. $Q^{\text{pb}} = Q_k^{\text{tes}}$) the amount of work produced is:

$$w_k = \frac{Q_k^{\text{tes}}}{\eta_{\text{pb}}} \quad (23)$$

where

$$Q_k^{\text{tes}} = \begin{cases} Q^{\text{pb}} & \frac{s_{k-1}}{\Delta t} + Q_k^{\text{rec}} > Q^{\text{pb}} \\ \frac{s_{k-1}}{\Delta t} + Q_k^{\text{rec}} & 0 < \frac{s_{k-1}}{\Delta t} + Q_k^{\text{rec}} \leq Q^{\text{pb}} \\ 0 & \text{otherwise} \end{cases} \quad (24)$$

and Q^{pb} is the thermal input required to run the power block at rated load, s_k is the stored thermal energy, and Q_k^{rec} is the thermal energy coming from the receiver(s). The thermal storage charge is calculated as

$$s_k = s_{k-1} + (Q_k^{\text{rec}} - Q^{\text{tes}}) \cdot \Delta t \quad (25)$$

The charge state is constrained to the maximum storage charge, s^{max} of the TES. When the maximum charge is reached the heliostat-field will partially or fully defocus to limit the amount of energy into the thermal storage depending upon its current and maximum capacity, as shown in (26):

$$Q_k^{\text{rec}} = \begin{cases} Q_k^{\text{rec}} & \frac{s_{k-1}}{\Delta t} + Q_k^{\text{rec}} < \frac{s^{\text{max}}}{\Delta t} \\ \frac{s^{\text{max}} - s_{k-1}}{\Delta t} & \frac{s_{k-1}}{\Delta t} + Q_k^{\text{rec}} > \frac{s^{\text{max}}}{\Delta t} \\ 0 & \frac{s_{k-1}}{\Delta t} \geq \frac{s^{\text{max}}}{\Delta t} \end{cases} \quad (26)$$

Thermal energy from the receiver is the sum of several arrays each with their own heliostat field and receiver system. Let there be L arrays and $\ell = 1, 2, \dots, L$ be the array index for all solar towers. The total receiver energy output from all arrays is therefore calculated as the sum from each

array:

$$Q_k^{\text{rec}} = \sum_{\ell=1}^L Q_{k,\ell}^{\text{array}} \quad (27)$$

Receiver array energy output, Q^{array} is subjected to a constant receiver thermal energy loss, Q^{loss} as such the contribution from each tower array is subjected to:

$$Q_{k,\ell}^{\text{array}} = Q_{k,\ell}^{\text{field}} - Q^{\text{loss}} \quad (28)$$

Receiver saturation and deprivation conditional requirements are introduced to improve the receiver model. Saturation conditions occur when the incident receiver thermal energy is greater than the operating capacity, for modelling purposes the receiver power is capped at the maximum design point, Q^{max} . Receiver deprivation conditions are met when the incident thermal power is less than the constant thermal losses of the receiver, the receiver is turned off and the energy output is set to zero during these conditions. It is assumed that when the receiver is operating in a restricted capacity either from storage constraints, receiver saturation or deprivation the heliostat fields will defocus by adjusting their azimuth angle to redirect DNI off the receiver while maintaining the correct tilt angles. In addition to the constraints of Eqs 26 the aforementioned constraints must also comply for each array:

$$Q_{k,\ell}^{\text{array}} = \begin{cases} Q_{k,\ell}^{\text{field}} - Q^{\text{loss}} & Q^{\text{loss}} < Q_{k,\ell}^{\text{array}} \leq Q^{\text{max}} \\ Q^{\text{max}} - Q^{\text{loss}} & Q_{k,\ell}^{\text{array}} > Q^{\text{max}} \\ 0 & Q_{k,\ell}^{\text{field}} \leq Q^{\text{loss}} \end{cases} \quad (29)$$

Reflected DNI received by each array from their respective heliostat fields are calculated with:

$$Q_{k,\ell}^{\text{field}} = \text{DNI}_k \sum_{j \in \mathcal{J}_\ell} A_j^{\text{total}} \cdot \eta_{k,j}^{\text{opt}} \cdot \hat{\rho}_{k,j} \quad (30)$$

where DNI_k is the incident DNI, \mathcal{J}_ℓ is the set of representative heliostats (i.e.) sector that are targeted at receiver ℓ , A_j^{total} is the sum of reflective area for heliostat sector j , and the $\eta_{k,j}^{\text{opt}}$ is the mean product of heliostat cosine, attenuation, blocking, shading, and image intercept efficiencies of all heliostats in sector j at time index k .

2.2.1. Simulating Heliostat Reflectance with Cleaning

For each time step, the soiling state of each representative mirror is updated by adding the current soiling rate to the cumulative particle number distribution. When a cleaning event occurs a *reflectance recovery* (i.e. cleaning) model is utilised to determine the total number of particles removed from the cleaned heliostat. Let $N_{k,j}(D)$ be the cumulative number of particles on the mirror before a cleaning action and $N_{k+1}(D)$ be the remaining particles just after a cleaning event. The reflectance recovery model is given as:

$$N_{k+1,j}(D) = \begin{cases} n_{k,j}(D) + N_{k,j}(D)(1 - \eta_{cl}(D)) & \mathcal{D}_{k+1,j} = 1 \\ n_{k,j}(D) + N_{k,j}(D) & \mathcal{D}_{k+1,j} = 0 \end{cases} \quad (31)$$

where $0 < \eta_{cl} \leq 1$ is the cleaning efficiency (i.e. the fraction of particles that are removed at D) for a particular cleaning technology and \mathcal{D} is the cleaning decision that is given for a particular cleaning schedule.

Initial reflectances of each representative heliostat should be specified. It is desirable to set these reflectances so that the initial and final conditions are the same — thus producing a “steady-state” reflectance trajectory. This steady-state condition ensures that the initial soiling state of the heliostats are aligned with typical soiling status of a plant at the start of the year (not perfectly clean). To achieve this, a boundary condition check for each representative heliostat is conducted after running the cleaning model. If there is a substantial difference between $N_{1,j}$ and $N_{K,j}$ the cleaning model is repeated using the initial conditions of $N_{1,j} = n_{1,j} \cdot \Delta t + N_{K,j}$ for the given cleaning schedule. After a set tolerance is reached, predicted reflectance values for each heliostat sector are computed using (11) and (12).

3. Case Study: A 50 MW Modular CSP Plant

NWQHPP (lat = -20.732° lon = 139.384°) is a prospective 50 MW solar hybrid baseload power plant integrating gas turbine, PV, modular CSP + TES technology to provide continuous utility scale power production for Queensland’s rural North West Power System grid. Cleaning resources for the heliostat field have been optimised using the presented FFTBCS heuristic and modified DSM for an early design of the CSP plant. The degradation costs were computed as the average of multiple weather trajectories to estimate the *expected* degradation costs. This averaging will prevent over-specialization of the cleaning schedule to one single dust trajectory and instead prefer those

that lower the average over a range of plausible conditions.

3.1. Experimental Measurement Campaign

The experimental set-up is comprised of a weather monitoring station and a mirror test rig, as shown in Fig. 3. The weather station measured key environmental parameters required to predict soiling losses using the DSM. TSP, wind speed and ambient temperature were recorded from the weather station over a two-year period. A solar mirror test rig was assembled near the weather station (within 20 m) and was used to fasten solar mirrors at a fixed tilt angle and aid in the retrieval of reflectance measurements over a period of time. The test rig was comprised of 18 mirror samples each tilted at various fixed angles (5° , 30° , 60° , and 85° with respect to the horizon) and repeated for each orientation (North, East, South, West) in addition to a vertical East facing and a horizontal mirror on the the North arm of the test rig.

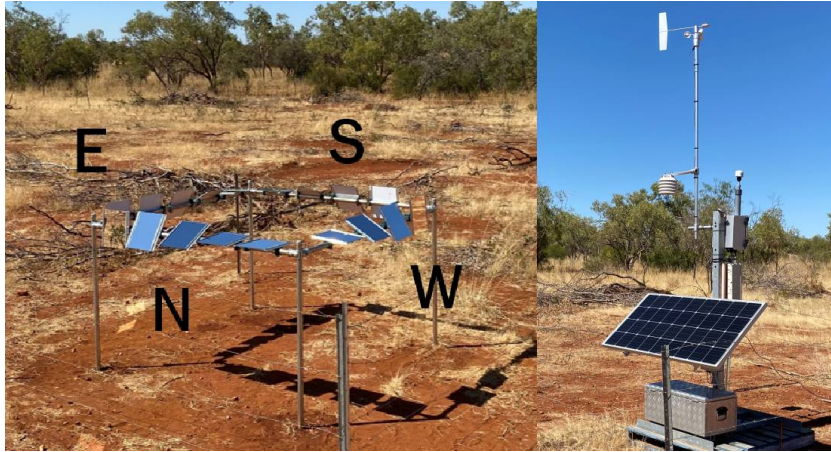


Figure 3: (Left) Mirror test-Rig; and (Right) TSP, temperature, relative humidity, and wind speed weather station

3.1.1. Airborne Dust Characteristics

The TSP was measured using an Ecotech eSampler with a one-second sampling rate, and the data was averaged every five minutes over a two-year period. The instrument employs a forward light scatter laser Nephelometer to measure TSP concentrations ranging from 0 to 65 mg m^{-3} , with a

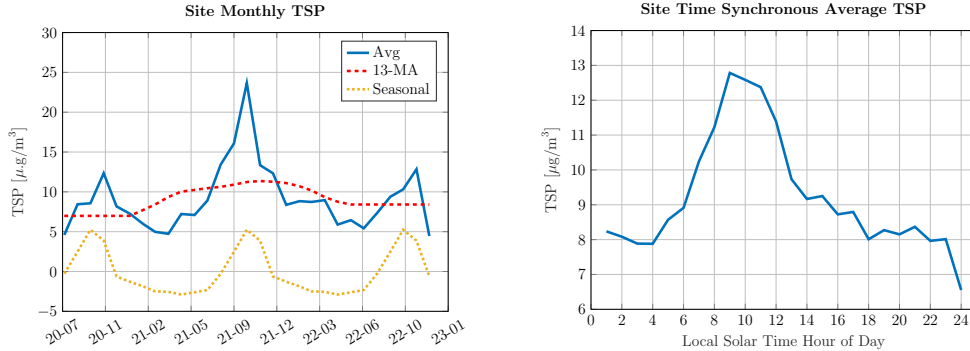


Figure 4: Left: Monthly averaged site TSP with 2x12 moving average (MA) filter and stable seasonal component. Right: Solar time synchronous average total suspended particle count.

reported precision of $3 \mu\text{g m}^{-3}$ or 2% (whichever is greater) and a resolution of $1 \mu\text{g m}^{-3}$.

The measurements revealed a mean TSP concentration of $9.1 \mu\text{g m}^{-3}$, with a standard deviation of $14.9 \mu\text{g m}^{-3}$ and a peak of $1075 \mu\text{g m}^{-3}$. Analyzing the two years of data using an additive decomposition time series model [32], evidence of cyclic seasonality was observed. The mean monthly TSP concentrations showed an increase of approximately $5 \mu\text{g m}^{-3}$ in October and a decrease of $3 \mu\text{g m}^{-3}$ in May each year, as shown in Fig. 4 (left).

Additionally, Fig. 4 (right) presents the intraday solar time synchronous average TSP. The intraday TSP levels were higher during CSP operational times (7 to 19) and decreased during the night.

3.1.2. Cleanliness Measurements

Mirrors were cleaned with demineralized water and a squeegee to measure the nominal clean reflectance values using a D&S Portable Specular Reflectometer (15R-USB, S/N: 713). Four reflectance measurements were made for each mirror, one at the centre of each quadrant, with measurements of each mirror being recorded. Following the initial set of measurements, the reflectance of all mirrors were measured twice a day over a seven day period in September 2020. The reflectometer was configured to measure specular reflectance with the instruments white LED at an incidence angle of 15° with an acceptance half angle of 12.5 mrad . For the duration of the measurement campaign there was no additional mirror cleaning from either manual labor or rain. All reflectance measurements were converted to a ζ ratio using (32),

where $\rho_{0,j}$ is the mean initial clean reflectance of mirror j .

$$\zeta = \frac{\rho_{k,j}}{\rho_{0,j}} \quad (32)$$

Fig. 5 shows the mean cleanliness for each tilt angle when considering all orientations. Results show that the soiling rate³ decreases with increasing tilt angle, where the horizontal mirror (0°) experienced higher soiling rates of 0.4 pp/d relative to the near vertical tilted (85°) mirrors of 0.02 pp/d. Mean cleanliness values for each orientation are shown in Fig. 6, the mean is calculated using the cleanliness values from the 5, 30, 60, and 85° tilted solar mirrors of each orientation. Soiling rates for each orientation are similar with the means being within the standard deviations of each other, as such for soiling rate predictions it is assumed that soiling rates are independent from heliostat azimuth angles.

3.1.3. Ground soil composition

Main components of the local soil were determined by collecting two samples of dust from the ground in proximity of the mirror test-rig (as a proxy to the airborne dust components). The samples were analysed with an XRD technique at the CARF within QUT. Results showed the main crystalline phase is represented by Quartz (SiO_2) which accounts for 40 to 47 % by weight in addition to 12 to 21 % by weight of amorphous content. This is in accordance with the assumption adopted in the DSM that dust is assumed to be silica with a density of 2000 kg m^{-3} .

3.1.4. Soiling Model Parameter Fitting and Predictions

The reflectance measurements and weather station measurements were used to estimate the free parameter h_r/z_o of the DSM. It should be noted that the 0° and 90° tilted mirrors have been excluded from the fitting procedure as they only exist on the North and East axis respectively. Table 1 shows the MSE and soiling rates for all tested fixed tilt angles. The fitted MSE shows excellent agreement between predicted and measured reflectance values, although this is facilitated by the accurate knowledge of the initial reflectance value which may not be available for every heliostat in the field.

Table 1 also shows the fitted h_r/z_o values using the mean reflectance

³Soiling rate is the change in cleanliness as a percentage over a period of time

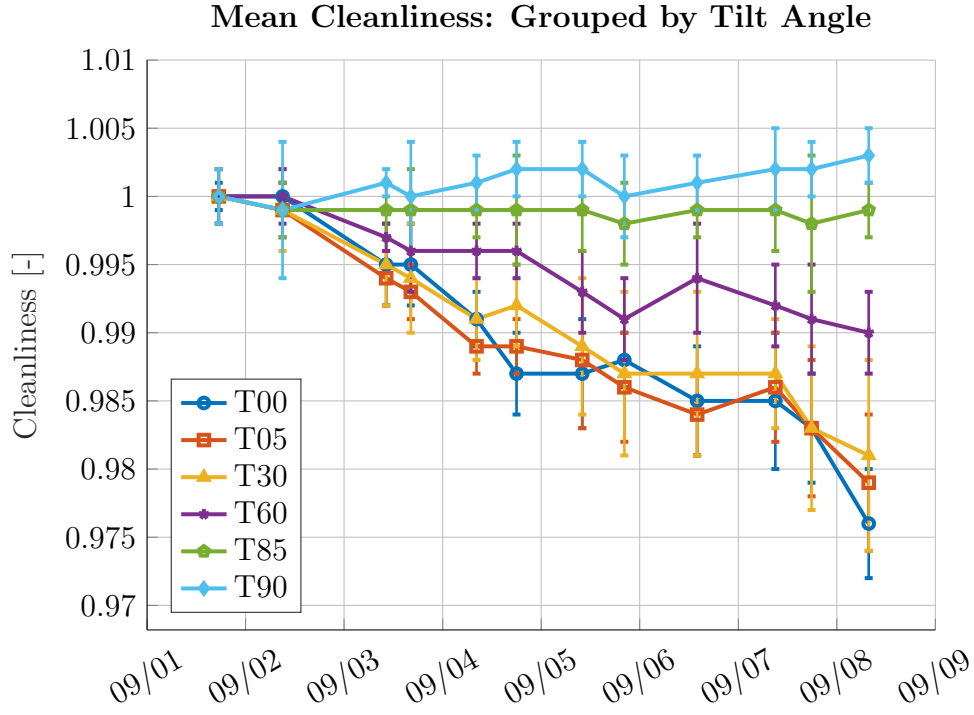


Figure 5: Mean cleanliness of all orientations with respect to mirror tilt angle (T)

for each of the tested tilt angles. According to literature [33] the surface roughness for a scrub or open area is $z_0 \approx 0.2$ m and $z_0 \approx 1$ m for tree covered areas (which is representative of the surrounding environment at the Mount Isa site). Considering the reference wind measurement height of $h_r = 3$ m, h_r/z_0 should be within 3–15. Thus the fitted and mean h_r/z_0 values reported are consistent with this back-of-the-envelope analysis and future predictions will use the mean h_r/z_0 of 5.8. Though there is a modest trend between tilt angle and h_r/z_0 values it will be assumed to be constant and the topic of future studies. With the fitted h_r/z_0 the DSM can be used to predict soiling losses for not only the fixed tilt mirrors at the Mount Isa site, but also for hypothetical heliostats that follow a receiver aiming strategy. An example of future soiling loss predictions of a fixed 30° mirror is given in Fig. 7.

The predicted soiling rates are shown in Fig. 8 for the low and high TSP seasons identified in Fig. 4 left for a 0° tilted fixed mirror. With the high

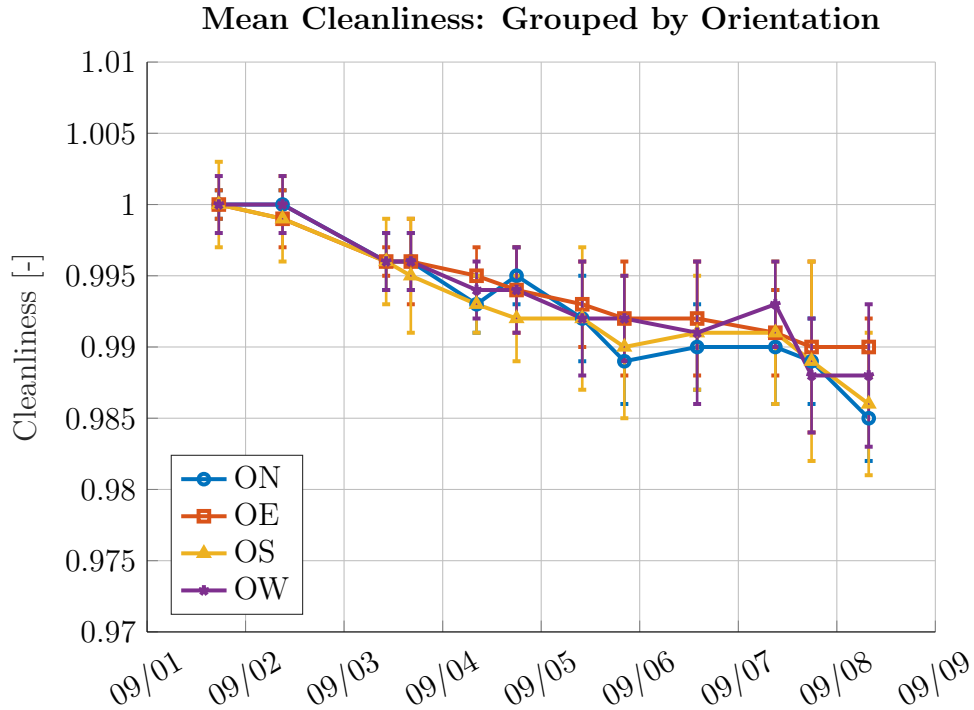


Figure 6: Mean cleanliness of tilt angles (5, 30, 60, 85) with respect to orientation (North - ON, East - OE, South - OS, West - OW)

season defined as the period where the mean seasonal TSP is above 0 and low being below that. High season soiling rates have a higher mean of 0.22 pp/d and variance relative to the 0.12 pp/d low season. Note that predicted high seasonal soiling rates are lower than that reported in Table 1 during the experimental campaign (0.35 pp/day) as measurements were carried near the peak of the high season.

3.1.5. Extension and Sampling of Meteorological Trajectories

Soiling rate predictions and optimization of cleaning resources require long-term meteorological data. However, the available meteorological data from the Mount Isa CSP site covers just over two years, which is insufficient for optimizing cleaning resources under various meteorological scenarios. To address this limitation and extend the TSP and wind speed time series to a full ten years, the time series analysis approach detailed in section 2.1.1 was

Table 1: Mean squared error, predicted and experimental soiling rates, and fitted h_r/z_o for all tilt angles

Tilt (°)	MSE (%)	Predicted SR (pp/d)	Experimental SR (pp/d)	h_r/z_o
0	3.4	0.35	0.40	-
5	2.3	0.33	0.33	6.6
30	1.2	0.29	0.30	5.9
60	1.3	0.17	0.17	5.7
85	0.26	0.003	0.002	5.0

employed.

By utilizing Akaike’s Information Criterion, an AR(24) TSP model and an AR(9) wind speed model was selected. Fig. 9 provides a preview of the simulations. Comparing the mean values and shape characteristics of the site measurements with the AR simulations revealed sufficient agreement to justify extending the meteorological trajectories.

Temperature recordings for the ten year trajectories were made up of the original two years of measurements and extended using a Mount Isa city measurement station, as both stations recorded similar values across the same time frame. Eight years of historical temperature data was used to impute the remaining temperature trajectories.

DNI estimates from satellite imagery between 1989 and 2015 were sourced from the Bureau of Meteorology (BOM). The data was split and grouped by day of year, such that for each day of the year there were 26 days of hourly DNI recordings. For each trajectory and simulation day of year random hourly trajectories were drawn from the grouped data to impute the simulation year.

3.2. CSP Plant Configuration

3.2.1. Plant Design Parameters

The CSP plant used for the case study is a 56 MW facility, integrated with a 14.5-hour thermal storage system and connected to a steam turbine with a similar capacity. The plant’s thermal storage is designed to be charged by 30 polar square solar field-arrays, each consisting of 2389 heliostats per array. These heliostats are strategically positioned to efficiently harness Direct Normal Irradiance (DNI) and focus it towards a $Q^{\max} = 10$ MW receiver

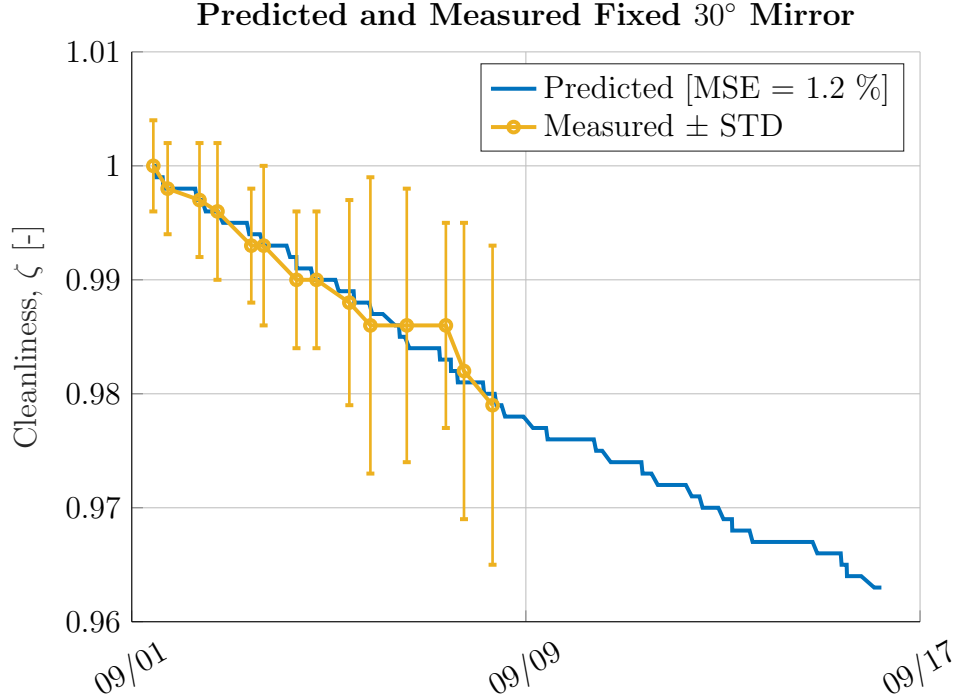


Figure 7: Predicted and measured cleanliness of a 30° tilted mirror using $h_r/z_o=5.8$ and site meteorological data

system.

During operation, the receiver system maintains a constant thermal loss of $Q^{\text{loss}} = 0.91$ MW. The CSP plant operates when solar zenith angles are below 80°, and the thermal receiver power exceeds the constant thermal receiver losses. The electrical power generation is assumed to run with a steady thermal-to-electricity efficiency of $\eta_{\text{pb}} = 35\%$. The parameters required for the cleaning optimization process are outlined in table 2.

Each array's solar field is assumed to have the same layout as shown in Fig. 10. To reduce computational load each solar field was sectorised into a 55x4 grid with one representative heliostat per sector. Four representative heliostats were chosen for each of the fifty five cleaning corridors⁴ based upon an even displacement position within the corridor.

⁴Cleaning corridor is defined as the South to North route taken by cleaning crews to clean heliostats

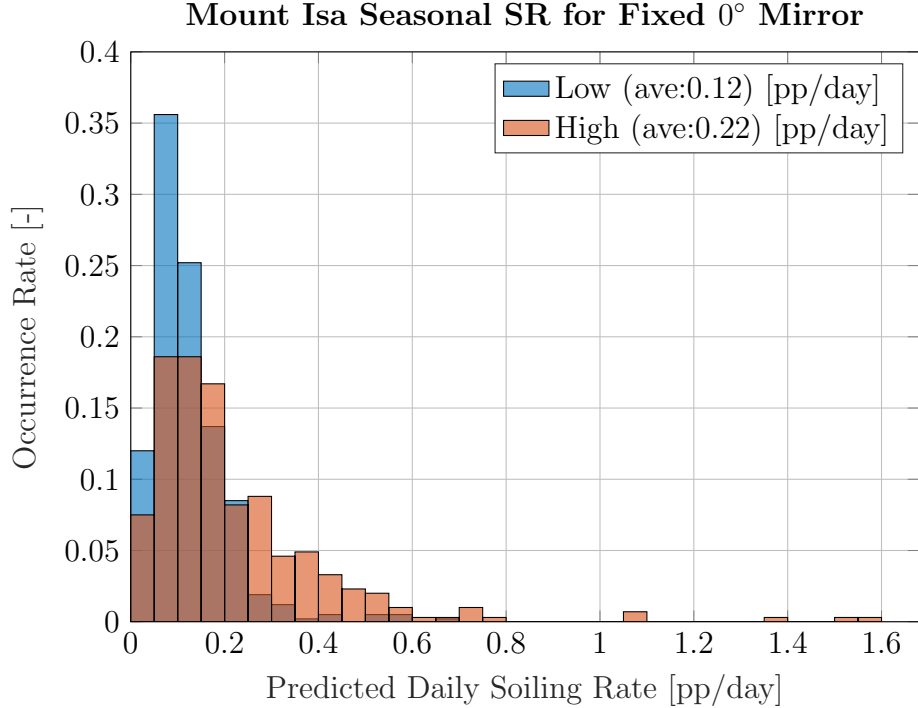


Figure 8: Mount Isa site predicted seasonal soiling rate for a 0° fixed-tilt angle mirror with $h_r/z_o = 5.8$, high season between August and December, and low season between January and June.

SolarPILOT-v1.5.2 ([34]) was used to generate an optical efficiency look up table using the receiver design characteristics and heliostat field position for all feasible solar azimuth and zenith angles. Hourly optical efficiency values were interpolated for the simulated year using geographical coordinates of the site and the Michalsky [35] solar position algorithm. The optical efficiency was calculated for each heliostat of sector j and simulation period k and with the mean being used for the sector representative heliostat.

Hourly particle deposition rates, n from the fitted DSM across the ten meteorological trajectories were calculated using each representative heliostat’s hourly tilt and incidence angle computed from the Guo et al. [36] heliostat tracking algorithm. The resultant soiling rates of each sector representative were fed into the cleaning model of the cleaning optimizer to retrieve predicted reflectance trajectories for a given cleaning resource setup.

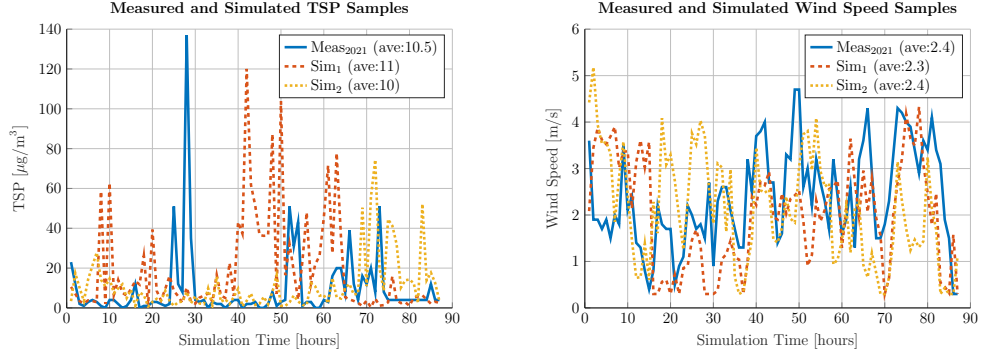


Figure 9: Left: TSP site data and AR(24) TSP simulation snapshots. Right: Wind speed site data and AR(9) wind speed simulation snapshots.

Table 2: CSP plant model values

Parameter	Value
Rated power block work, w^{rated}	56 MW
Power block efficiency, η_{pb}	35 %
Max storage charge, s^{max}	2320 MW h
Max receiver energy, Q^{max}	10 MW
Constant receiver loss, Q^{loss}	0.9 MW
Solar field arrays	30
# Heliostats per module	2389
Heliostat mirror area, A^{mirror}	6.4 m ²

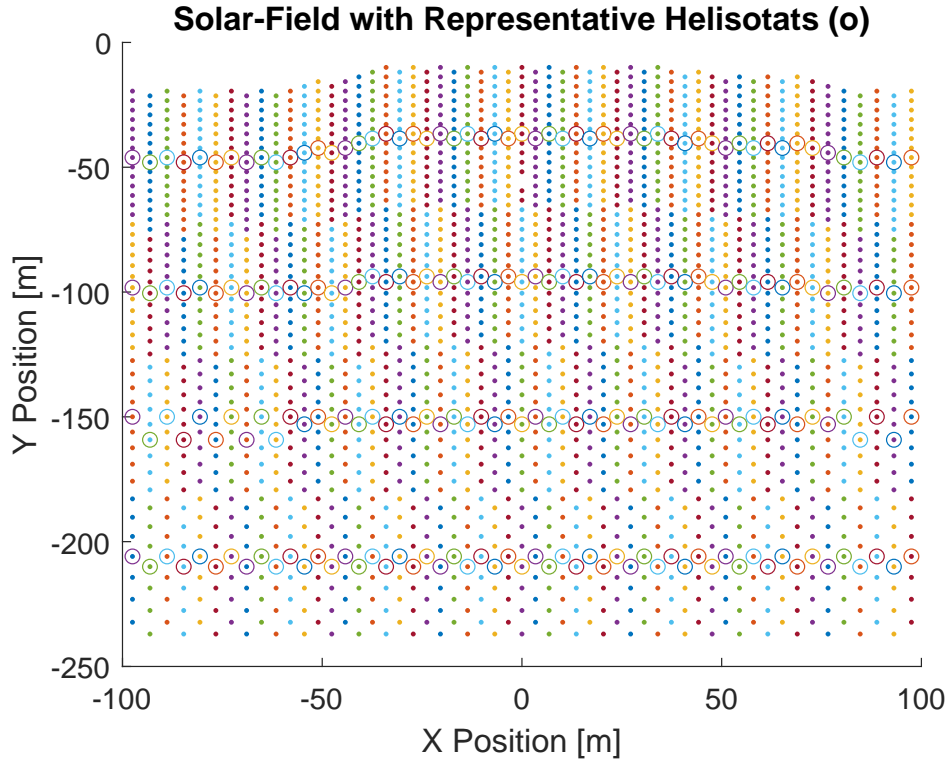


Figure 10: Solar field sectors with representative heliostats denoted as circle outlines, receiver centred at (0,0)

3.2.2. Cleaning Resource Parameters

Characteristics of the solar field geometry and operating conditions of the cleaning crew allow an estimation of the cleaning speed for a high pressure + brush operating cleaning crew. Assuming the crew cleans for 8 h per shift at an average vehicle cleaning velocity of 2 km h^{-1} and non-cleaning travel velocity of 10 km h^{-1} it is expected that one solar field will be cleaned per crew per shift (heliostat area cleaning rate of $2039 \text{ m}^2 \text{ h}^{-1}$) which also includes return trips for breaks and reloading fuel/water at the start of the day.

For each cleaning event a crew will path through all cleaning corridors of a unique solar field, restarting the cleaning rotation once all heliostats of the power plant have been cleaned. Cleaning crews are comprised of one operator

Table 3: Cleaning and cost model values

Parameter	Value
Tractor velocity (cleaning)	2 km h ⁻¹
Tractor velocity (no cleaning)	10 km h ⁻¹
Tractor work load	82 kW
Operator shift time	8 h
Water consumption rate	0.4 L m ⁻²
Fuel consumption rate	25 L h ⁻¹
Cleaning efficiency, η_{cl}	99 %
Price of electricity, P	140 A\$/MWh
Plant O&M Costs, $C^{o\&m}$	3.5 A\$/MWh
Truck cost, C^{truck}	300 000 A\$/truck
Asset depreciation time, b	10 yr
Operator salary, C^{salary}	80 000 A\$/yr
Truck maintenance cost, C^{maint}	15 000 A\$/yr
Water and fuel costs, $C^{w\&f}$	0.0175 A\$/m ²

and a cleaning tractor⁵ with a high pressure spray and cleaning brush with 7 kL of water capacity. The high pressure wash and brush cleaning technology is assumed to remove $\eta_{cl} = 99\%$ of particles for all diameters.

3.2.3. Economic Assumptions

Determining the cleaning costs and soiling-induced-degradation costs requires economic assumptions about the cleaning crew, equipment, electricity and operation and maintenance costs for the power plant. These costs (see Table 3) include the tractor depreciation cost over the expected asset lifetime (C^{truck}/b), truck maintenance cost, Operator salary. Price of electricity, P of the plant has been assumed to be inline with the regions calculated cost of A\$140 MW⁻¹ h [38]. Non-cleaning operation and maintenance costs of the plant are assumed to be A\$3.5 MW⁻¹ h.

3.3. Operating Scenarios

The model parameters given in the previous section and ten meteorological trajectories have been combined with design and operating strategies to

⁵Fuel rate derived for 82 kW tractor [37]

investigate the effects on TCC. These operating scenarios include a base setup which will serve as a reference to compare against the three scenarios that change either the angle at which heliostats are stowed at night, dispatch policy, and the time at which heliostats are cleaned.

3.3.1. Base Setup

The base scenario is an operation strategy that assumes all thermal energy collected is converted into electricity as such the dispatch policy is the continuous production of available energy. Heliostats will have a near vertical park angle⁶ of 85° to limit soiling-induced reflectance loss when not in operation. In addition, all cleaning events are assumed to occur instantaneously at midnight.

3.3.2. Horizontal Park Setup

Heliostats are often parked in the horizontal position to reduce wind loads. By decreasing wind loads the costs associated with structural supports and maintenance (i.e. alignment calibration) may be lowered. To better understand the soil degradation costs associated with this operational mode a scenario has been setup to park heliostats in a horizontal position (0° tilt) during night time stowing.

3.3.3. Night Dispatch Setup

The Mount Isa regional electrical grid is connected to several large mines and production facilities requiring continuous electrical demand. For the night dispatch scenario it is assumed that during the day the TES is filled while the PV fields provide continuous power generation below zenith angles of 80°, at which point the PV field is turned off⁷ and the TES begins providing thermal energy for the power block. As such the dispatch policy of (24) are modified to also include SZA night time dispatch constraints:

$$Q_k^{\text{tes}} = \begin{cases} Q^{\text{pb}} & \frac{s_{k-1}}{\Delta t} + Q_k^{\text{rec}} > Q^{\text{pb}} \ \& \ \text{SZA}_k > 80 \\ \frac{s_{k-1}}{\Delta t} + Q_k^{\text{rec}} & 0 < \frac{s_{k-1}}{\Delta t} + Q_k^{\text{rec}} \leq Q^{\text{pb}} \ \& \ \text{SZA}_k > 80 \\ 0 & \text{otherwise} \end{cases} \quad (33)$$

⁶Park angle is defined as the tilt angle of the heliostat when stowed

⁷This is a simplification of how the PV and gas power plants will provide power. In reality a combination of thermal storage capacity and available PV power would decide when to operate the power block

3.3.4. Day Cleaning Setup

In the previous scenarios cleanings are assumed to occur instantaneous at midnight. However, heliostats are generally cleaned during the daytime when operators can maneuver cleaning vehicles in tight clearances around heliostats in visible conditions. The downside of this cleaning strategy is the lost productivity from parking the heliostats in a vertical position while they are being cleaned. This scenario has been setup to investigate the effects of day time cleaning on the optimized cleaning strategy.

With 55 corridors cleaned per shift per crew (working time from 8 A.M to 4 P.M), it would take $T_c = 0.146$ h to clean one corridor. When a corridor is cleaned it is assumed to be parked for two cleaning passes. The first pass to clean the corridor and the second pass to allow enough clearance to clean the neighbouring corridor. To account for the lost productivity, heliostats will be assigned an uptime or productivity ratio per hour of operation; denoting the percentage a heliostat is producing energy during an hour of cleaning. As such corridors will have an uptime ratio, U of $U_{k,j} = \frac{1-2 \cdot T_c}{1} = 71\%$ while being cleaned and $U_{k,j} = 100\%$ when not being cleaned.

To account for productivity losses from parking the heliostats in the daytime, the reflected DNI from (30) is replaced with:

$$Q_{k,\ell}^{\text{field}} = \text{DNI}_k \sum_{j \in \mathcal{J}_\ell} A_j^{\text{total}} \cdot \eta_{k,j}^{\text{opt}} \cdot \hat{\rho}_{k,j} \cdot U_{k,j} \quad (34)$$

The C^{op} or profit loss due to parking the heliostats during the day is calculated as:

$$C^{\text{op}}(M, F) = (P - C^{\text{o\&m}}) \sum_{k=1}^K \left(w_k^{\text{clean}} - w_k^{\text{dayC}} \right) \Delta t \quad (35)$$

where w^{clean} is the work produced with an always clean heliostat field and no heliostat daytime parking losses (i.e. $U = 100\%$) and w^{dayC} is the work generated with an always clean heliostat field with consideration of day time cleaning parking (i.e. $U_{k,j} = 71\%$ for $\mathcal{D}_{k,j} = 1$).

The total cleaning cost of (20) is ammended to include the operational downtime cost

$$\text{TCC} = C^{\text{deg}} + C^{\text{cl}} + C^{\text{op}} \quad (36)$$

Table 4: Optimal cleaning schedules, mean work produced with a clean and soiled field, and mean costs associated for scenarios horizontal stowing (HS), night dispatching (ND) and day cleaning (DC)

	M	F	$w_{\text{rated}}^{\text{clean}}$ (MW h/yr)	$w_{\text{rated}}^{\text{soil}}$ (MW h/yr)	C_{cl} (kA\$/yr)	C_{deg} (kA\$/yr)	C_{op} (kA\$/yr)	TCC (kA\$/yr)
Base	2	24	202906	199948	452	404	0	856
HS	3	36	202906	198702	678	574	0	1252
ND	2	24	198018	196008	452	274	0	727
DC	2	24	202408	199484	452	399	68	919

3.4. Optimal Cleaning Resources

The soiling prediction and stochastic cleaning resource heuristic has been implemented using the NWQHPP design conditions for the four operating scenarios. Table 4 summarizes the optimal cleaning resource setup, electricity generated under clean and soiled fields and costs associated for each operating scenario. Optimal cleaning resource allocations for all near vertical stow angled scenarios occurs with two cleaning crews operating at the maximum cleaning rate of 24 cleans per year. While the optimal cleaning resources are similar, the difference in total cleaning costs is where each operating scenario differs. Contrastingly, horizontally stowed heliostats experienced the highest soil degradation cost and required the largest cleaning fleet with three crews cleaning each heliostat 36 times per year due to the increased soiling losses. Making the operating strategy one of the most costly in terms of soiling-based production loss.

3.4.1. Base Scenario Evaluation

The mean total cleaning cost are shown in Fig 11. Using the cleaning optimizer the optimal solution occurs with two crews cleaning all heliostats 24 times per year with a total cleaning cost of $TCC(2, 24) = A\$856\,000\text{ yr}^{-1}$.

Fig. 12 shows the total cleaning cost split between mean degradation and cleaning costs. Variations between degradation curves are minimal and increasing the number of field cleanings creates an exponentially decaying cost relation. Whereas, cleaning cost show a linear trend with each additional crew requiring a larger fixed cost and additional field cleanings will increase variable costs. As such surpassing the optimal cleaning resource setup will increase plant productivity but due to higher cleaning costs any production

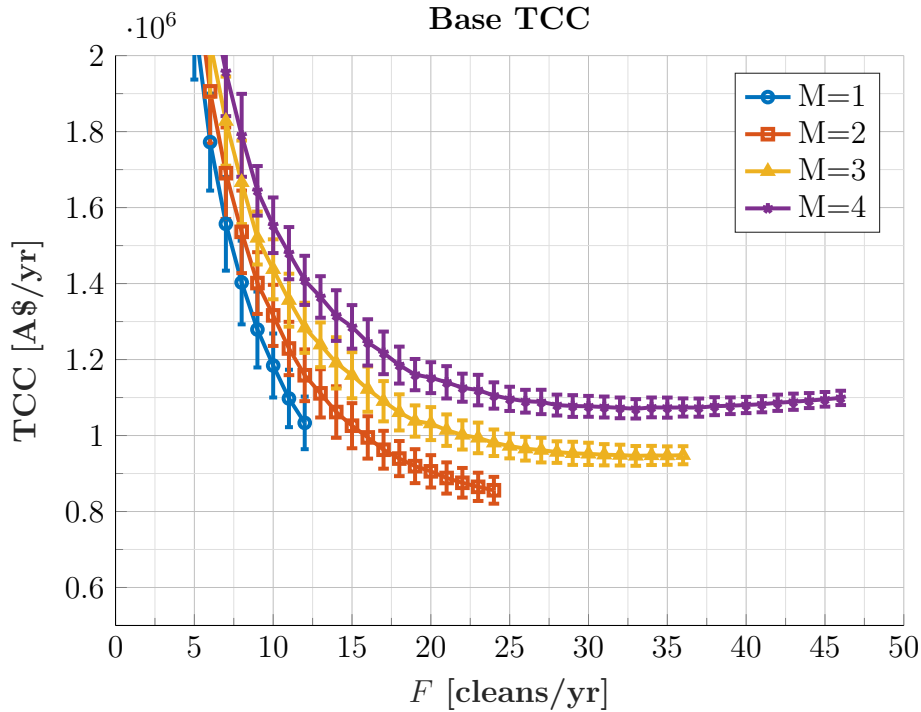


Figure 11: Base scenario mean annual total cleaning cost for different quantities of cleaning crews (M)

benefits are no longer economically efficient.

3.4.2. Cleaning Cost Breakdown

The breakdown of costs associated with one cleaning crew operating at the maximum cleaning rate⁸ is depicted in Fig. 13. It is evident that fixed costs outweigh variable costs, with salaries constituting the majority of yearly fixed expenses, accounting for 35% of the total cleaning costs. A smaller proportion of fixed costs is attributed to capital investment and maintenance of the cleaning vehicle itself.

Notably, with the ongoing advancements in automated cleaning vehicles [39, 40], a reduction in salary costs per cleaning crew is expected, as a single supervisor may oversee a fleet of automated vehicles. This potential

⁸The maximum cleaning rate corresponds to one crew cleaning each heliostat 12 times per year, with two crews able to clean each heliostat 24 times per year, and so on.

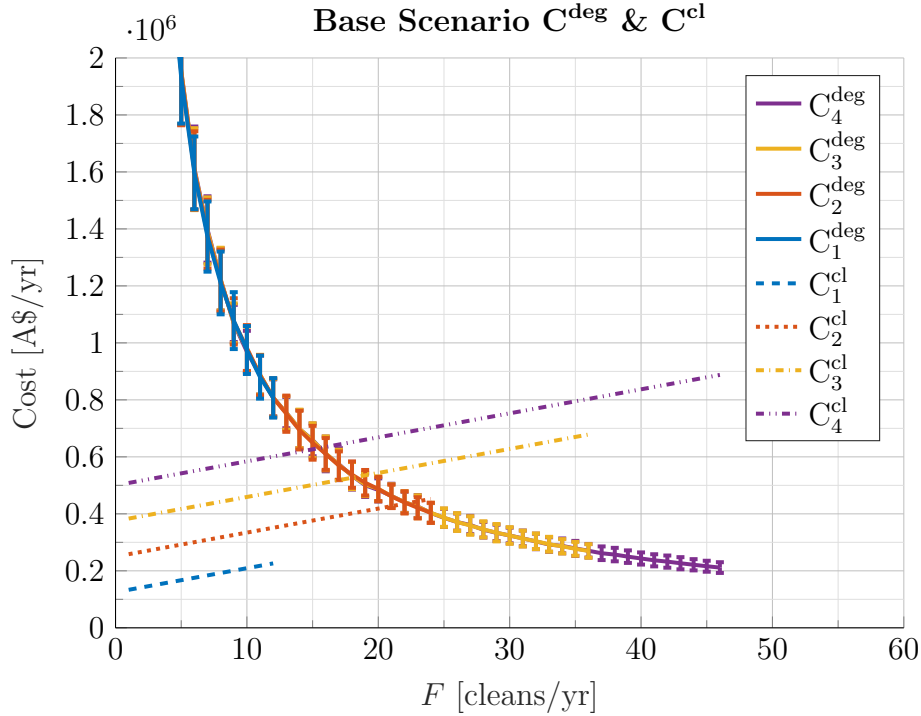


Figure 12: Base scenario mean annual degradation (C_M^{deg}) and cleaning costs (C_M^{cl}) for different amounts of cleaning crews (M)

shift would come at the expense of higher vehicle costs. However, automated vehicles can work over a longer shift time and which may even reduce the total number of cleaning crews needed. As such this cost-trade off may be advantageous if the total fixed cost proves to be lower than that of the staffed cleaning crew presented in this study.

Variable costs contribute nearly as much towards the cleaning cost. Primarily due to the 67.5 kL yr^{-1} of fuel required to operate each truck leading to the the annual fuel cost of $\text{A}\$94\,500 \text{ yr}^{-1}$ per crew or 42 % of the cleaning costs; dominating all cost factors listed in both categories. Whereas, the 2.2 ML yr^{-1} of water contributes about $\text{A}\$6600 \text{ yr}^{-1}$ per crew (3 % of cleaning costs) of the variable costs and is the lowest reported for all cleaning cost factors. The results suggest the need to reduce fuel usage within cleaning vehicles. The possibility of hybrid or fully electric vehicles could prove to be a solution as cheap electrical energy could be supplied by the plant.

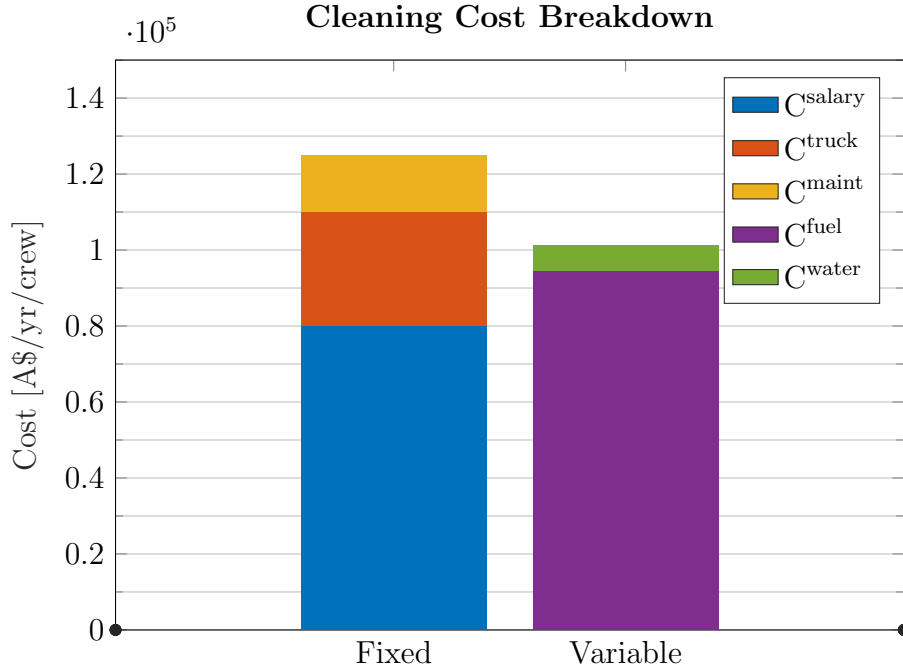


Figure 13: Cleaning cost breakdown for one cleaning crew operating at the maximum cleaning rate

3.4.3. Horizontal Stowing Evaluation

Stowing heliostats in a horizontal position will lead to higher soiling rates compared to vertical heliostats due to the increased soil deposition exposure and lower removal forces (see Fig. 5). Table 4 shows the total cleaning cost increased around $\text{A}\$400\,000\text{yr}^{-1}$ or 51% relative to the vertical stow results of the base scenario. Higher soiling rates even motivate the use of a third cleaning crew to reach the optimal cleaning schedule (see Fig. 14). Although, two cleaning crews is $\text{A}\$61\,000\text{yr}^{-1}$ more expensive and within the standard deviation of the three crew solution and may be adequate for low soiling trajectories.

The additional degradation cost associated with horizontally stowing the heliostats is approximately $\text{A}\$166$ per heliostat or $\text{A}\$25.9\text{m}^{-2}$ of reflective area, assuming a lifespan of 30 years. Considering heliostat prices of $\text{A}\$100\text{m}^{-2}$ [41], this results in a cost increase of 26% of the total heliostat price. Consequently, solar field designers should carefully weigh the economic benefits of reduced structural and maintenance costs due to wind loading against

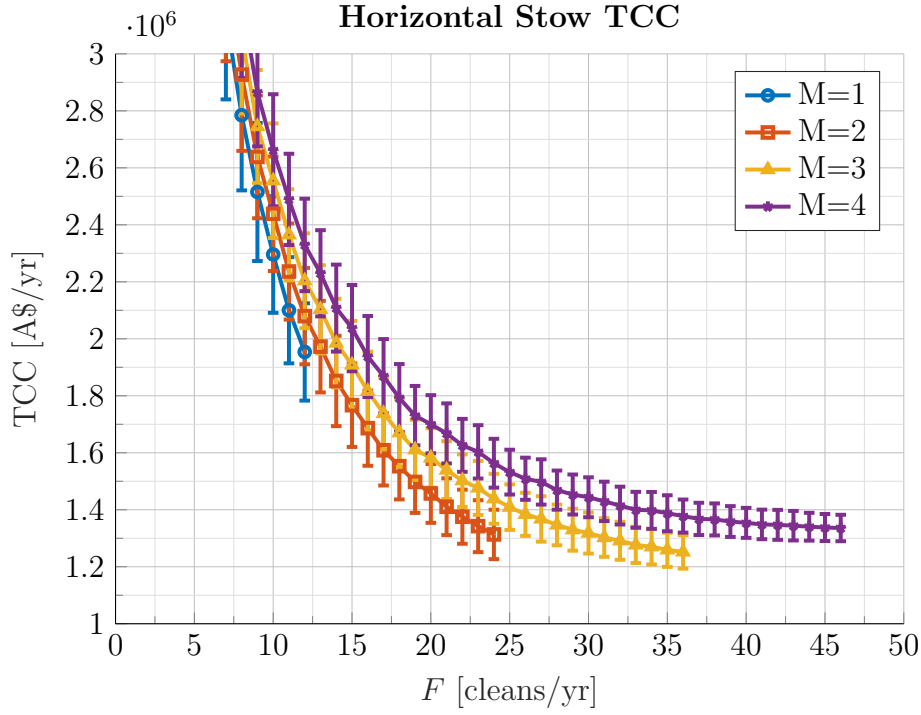


Figure 14: Horizontal stowing scenario mean total cleaning cost for various amounts of cleaning crews (M)

the additional expenses related to cleaning and productivity losses caused by soiling.

Soiling rates predicted from the DSM for all simulation periods are summed daily and averaged across each heliostat sector⁹ and shown in Figs 15 and 16 for both vertical and horizontal stow respectively. The plots suggest that horizontally stowed heliostats undergo higher daily soiling rates (0.15 pp/day) with respect to those vertically stowed (0.07 pp/day). Thus, an increase in daily soiling rates of 114%.

Both soiling rate maps show a relation between soiling rate and relative position within the solar field. Soiling rates tend to decrease with distance from the receiver; since heliostats close to the receiver have horizontally inclined tilt angles corresponding to higher soiling rates. Although mirrors

⁹All solar field arrays will experience similar soiling fluxes but differ due to their tilt angles

closer to the receiver will have higher soiling rates the resultant impact on optical performance is slightly compensated due to lower incidence angles and thus lower geometry factor values, as expressed in (3).

Additionally, for heliostats with the same Y position, daily soiling rates increase with increasing X position (i.e. further East). This is due to the intraday time synchronous average TSP (see Fig. 4 right) being slightly higher during the morning when eastern heliostats have lower tilt angles with respect to western heliostats aiming at the receiver.

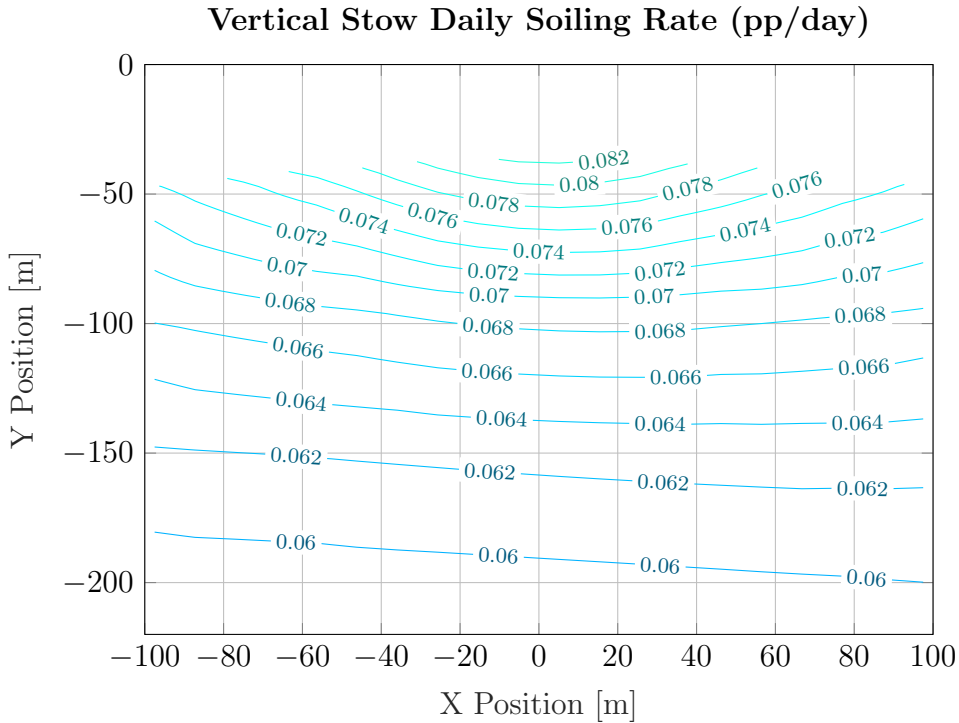


Figure 15: Mean daily heliostat field soiling rate (pp/d) interpolated in-between sector representatives for vertical stowing, receiver at (0,0)

3.4.4. Night Time Dispatching Only Evaluation

The night-time only dispatch policy introduces a night-time only CSP power block operation mode. Where PV energy provides day-time power while the CSP charges the TES; during the night the power block is run using the charged TES. Comparing the always cleaned power generation of

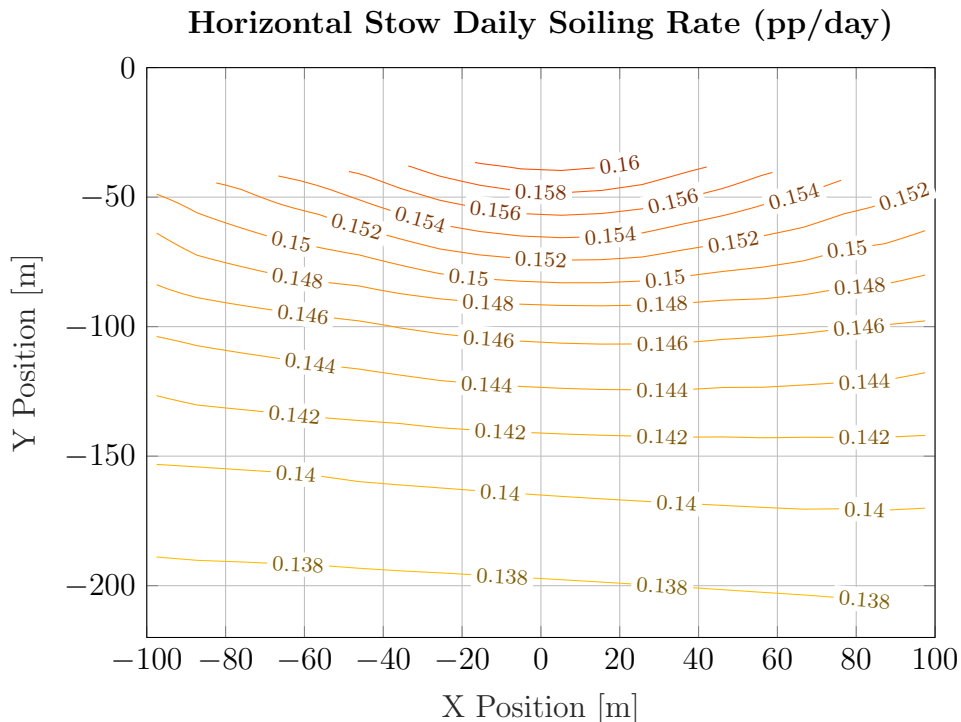


Figure 16: Mean daily heliostat field soiling rate (pp/d) interpolated in-between sector representatives for horizontal stowing, receiver at (0,0)

the night-time dispatch and base scenarios of table 4 shows that the night-time dispatch scenario produces less electricity than the base scenario. The difference is due to the receiver system turning off when the TES is filled, whose size is kept equal to the base case. Total cleaning costs plotted in Fig. 17 show an optimal cleaning setup with two cleaning crews cleaning the field 24 times per year.

In the night dispatch scenario, degradation costs are lower compared to the base case due to the introduced constraints on Thermal Energy Storage (TES) capacity. These constraints result in a reduced need for a perfectly clean solar field. The concept of "free" soiling also applies when the receiver operates in a saturated condition, where heliostats are defocused to prevent overheating of the receiver system. Figure 18 illustrates the excess energy lost due to operational constraints on the receiver and TES for both the base and night-time dispatch scenarios. Comparing the perfectly clean and soiled scenarios reveals that some of the energy reflected from a perfectly clean solar

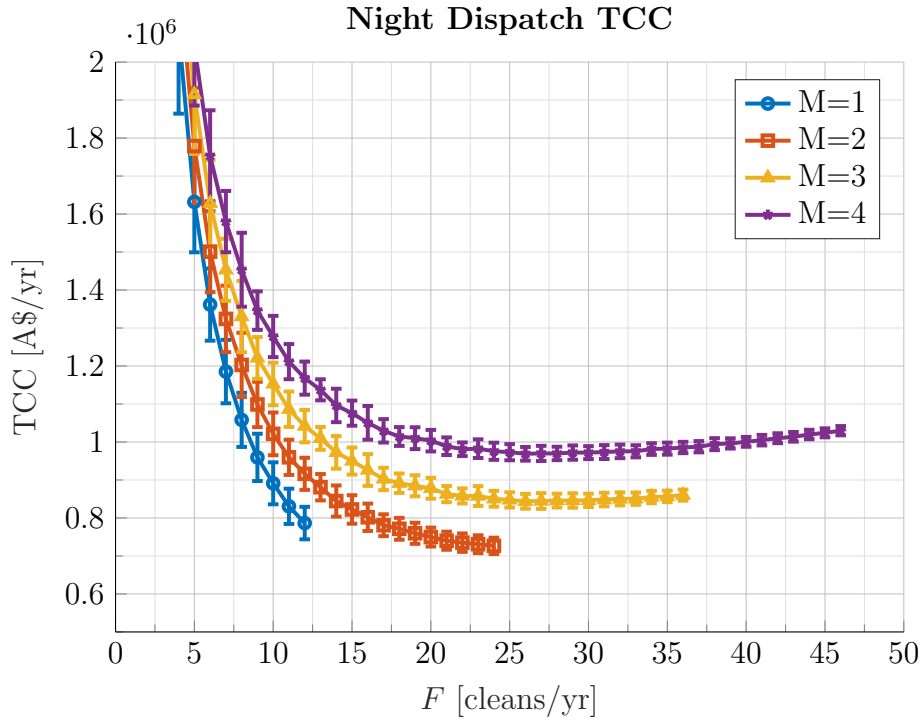


Figure 17: Total cleaning cost for night-time dispatching scenario

field is partially lost due to the storage and receiver saturation constraints. Consequently, the plant’s average yearly cleanliness, while meeting night-time production requirements, can be approximated as... [add the relevant approximation or further discussion here].

Degradation costs are notably lower in the night dispatch scenario compared to the base case, primarily due to the implementation of TES capacity constraints. These constraints effectively reduce the necessity for maintaining a perfectly clean solar field. Interestingly, the concept of "free" soiling also extends to instances when the receiver operates in a saturated condition, leading to heliostats being defocused to avoid overheating. Fig. 18 illustrates the excess energy lost due to operational constraints on the receiver and TES for both the base and night-time dispatch scenarios. By comparing the perfectly clean and soiled scenarios, it becomes evident that some of the energy reflected from a perfectly clean solar field is partially lost due to the storage and receiver saturation constraints. Consequently, it is possible to approximate the average yearly cleanliness that the plant can maintain and still fully

charge the storage as:

$$\zeta_{\max} = 1 - \frac{w_{\text{sat}}^{\text{clean}} + w_{\text{cap}}^{\text{clean}}}{w_{\text{rated}}^{\text{clean}}} \cdot 100 \quad (37)$$

where, ζ_{\max} is the yearly field average cleanliness corresponding to maximum production, $w_{\text{sat}}^{\text{clean}}$ is the work loss due to receiver saturation and $w_{\text{cap}}^{\text{clean}}$ is the work loss due to TES capacity constraints with an always clean solar field. As such, when operating with a night-time dispatch, a yearly field average cleanliness of 97.6% would allow for the TES to completely charge on most days.

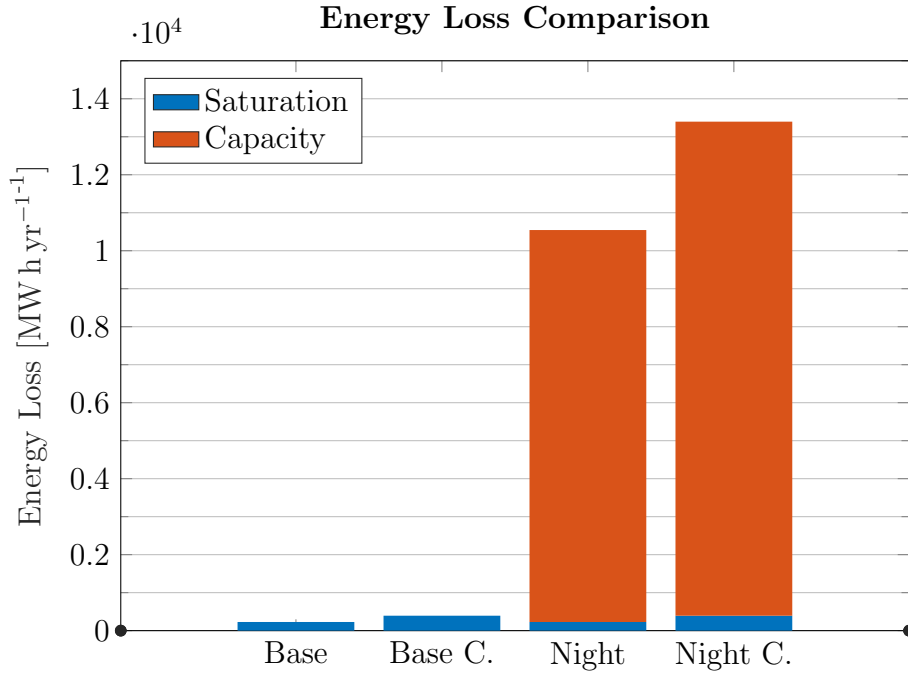


Figure 18: Thermal energy loss due to receiver and TES operational constraints during the base and night time dispatch scenarios for a soiled and cleaned (C) heliostat field

3.4.5. Day Time Cleaning Evaluation

Results from Table 4 show an optimal cleaning schedule occurs with two crews cleaning the solar fields 24 times per year (see Fig. 19). The effects of cleaning during the day can be seen when comparing the work produced by

an always clean solar field, where the base scenario produces 495 MW h more than the day cleaning policy. Interestingly, degradation costs are slightly lower due to the solar field being cleaner during production time. However the reduced heliostat up-time leads to higher operation costs that exceed any benefit of having a cleaner solar field during the day; incurring a total cleaning cost increase of 7% relative to a night-time cleaning policy. As such each crew contributes around A\$32 000 yr⁻¹ to the total cleaning cost making it a minor cost relative to other cleaning expenditures listed in Fig. 13.

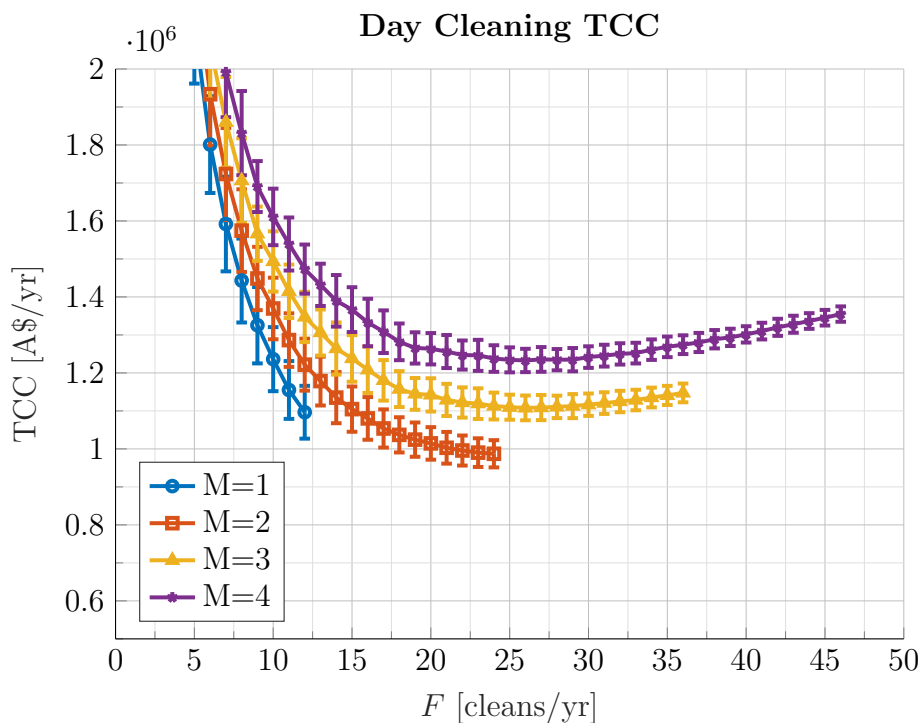


Figure 19: Total cleaning cost for day-time cleaning scenario

Operational downtime costs could be reduced through opportunistic maintenance such as cleaning during periods of downtime from insufficient solar energy, when the receiver is at saturated conditions or when the TES is fully charged and operating with a night time dispatch policy. Cleaning times could be adjusted to coincide with probable hours where a heliostat would not be producing energy to reduce total impact on productivity.

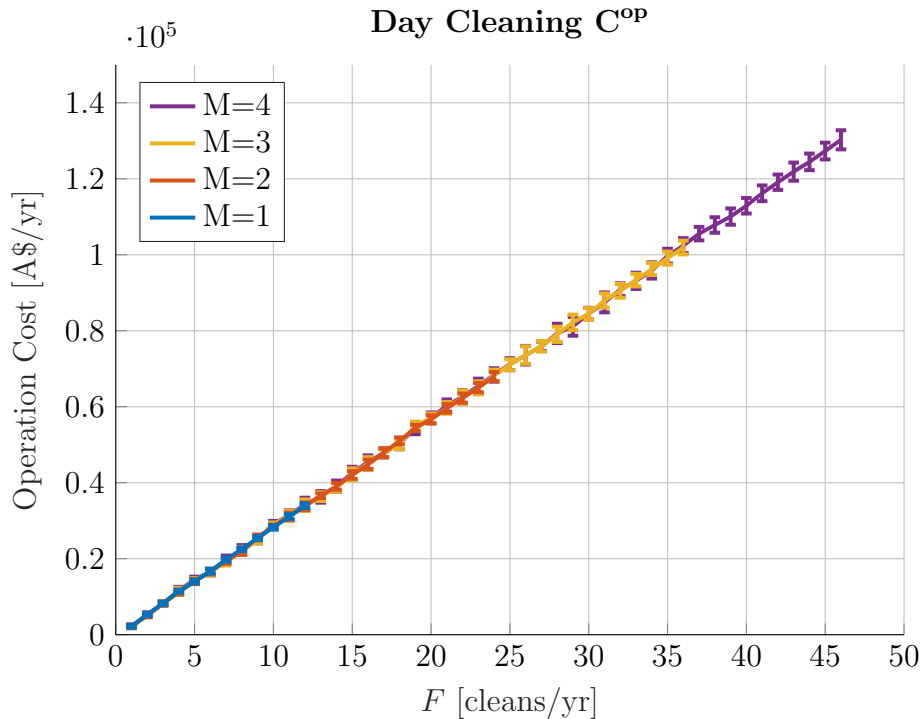


Figure 20: Day cleaning mean operational costs

4. Conclusion

Cleaning resources for a modular 50 MW CSP+TES were optimized early in the design phase using the developed soiling prediction and cleaning resource methodology. By calibrating the soiling model to the site through experimental measurements, mean soiling rates of 0.12 pp/d and 0.22 pp/d were predicted for the low and high dust season respectively. An autoregressive time-series model was used to extend two years of meteorological measurements into ten years allowing for multiple soiling trajectories to be evaluated. Additionally, usage of a second surface geometry model and updated receiver and thermal storage models allowed for an assessment of various CSP operation and design philosophies on soiling induced costs. The proposed methodology ultimately reduces financial uncertainty associated to soiling early in the design and site selection phases of a CSP plant.

For the base scenario utilizing vertically stowed heliostats and a continuous energy dispatch policy, an optimal cleaning schedule was found with two

crews cleaning the solar field 24 times per annum. A break down of cleaning costs showed that fuel and operator salaries contribute 42 % and 35 % of cleaning costs with a high pressure wash and brush cleaning crew.

The second scenario introduced a horizontally night-time stow operational policy. By stowing horizontally instead of vertically at night the soiling rate increased by 114 %. This led to hiring a third cleaning crew to reach the optimal cleaning schedule. Ultimately, the total cleaning cost and total lifetime cost of each heliostat increased by 51 % and 26 % relative to the base vertical stow scenario.

A night-time dispatch policy was explored, where during the day the modular CSP field would charge the TES for night time electrical production. Simulations showed that the oversized solar fields led to a large amount of energy loss due to maximum storage constraints on the TES system. The excess energy suggests that a daily fully-charged thermal storage could occur with a yearly field average cleanliness of 97.6 %, reducing the need to maintain perfectly clean solar fields.

A day-time cleaning scenario was setup to analyse the effect of shutting down groups of heliostats for cleaning during the day. Results showed that day-time cleaning incurred a productivity loss that increases linearly with the number of field cleanings per year. Resulting in a total cleaning cost increase of 7 % relative to the night-time cleaning policy. To minimize these costs it may be possible to perform opportunistic cleaning during periods where the receiver is operating in a saturated/depraved condition or when the thermal energy storage is full (assuming a night time only dispatch policy).

Acknowledgements

C.B. Anderson, G. Picotti, M.E. Cholette, and T.A. Steinberg acknowledge the support of the Australian Government for this study, through the Australian Renewable Energy Agency (ARENA) and within the framework of the Australian Solar Thermal Research Initiative (ASTRI Project ID P54). Additionally, the ground soil composition work was enabled by use of the Central Analytical Research Facility hosted by the Institute for Future Environments at QUT.

Appendix A. Overlap derivation

Heliostats operating at near normal incident angles can experience an overlapping of shading and blocking areas with the given second surface

geometry model. This overlapping of areas causes a reduction in the total obstructed area and can be corrected as a function of how overlapped the two regions are. As the blocking and shading areas are ellipses of the same size along one axis it is possible to use the overlap length, x_o to determine how overlapped the shaded and blocked areas are and analytically solve for the overlapping areas.

Consider the two ellipses shown in Fig. A.21 that are overlapped by length x_o , with a shared area denoted by A^{overlap} . Both shading and blocking ellipses can be parameterised with $(x, y) = (a \cos t, b \sin t)$, $0 \leq t \leq 2\pi$, where $2t = \bar{t}$. The eccentric anomaly, \bar{t} associated to the position of the overlap position relative to the ellipse length $a - x_o$ is derived as:

$$dx = -a \sin t dt \quad (\text{A.1a})$$

$$a - x_o = a \cos \bar{t} \quad (\text{A.1b})$$

$$\bar{t} = \cos^{-1} \left(\frac{a - x_o}{a} \right) \quad (\text{A.1c})$$

$$\bar{t} = \cos^{-1} \left(\frac{D - 2x_o \cos \theta}{D} \right) \quad (\text{A.1d})$$

so therefore, the overlapping area can be calculated as:

$$\frac{A_o}{2} = 2 \int_{a-x_o}^a y dx \quad (\text{A.2a})$$

$$= -2ab \int_{\bar{t}}^0 \sin^2 t dt \quad (\text{A.2b})$$

$$= 2ab \int_0^{\bar{t}} \sin^2 t dt \quad (\text{A.2c})$$

$$= ab (\bar{t} - \sin \bar{t} \cdot \cos \bar{t}) \quad (\text{A.2d})$$

$$A_o = 2ab (\bar{t} - \sin \bar{t} \cdot \cos \bar{t}) \quad (\text{A.2e})$$

$$A_o = \frac{D^2}{2 \cos \theta} \cdot (\bar{t} - \sin \bar{t} \cdot \cos \bar{t}) \quad (\text{A.2f})$$

The overlap length is equivalent to the difference between length \overline{BC} and \overline{ED} depicted in Fig. A.22. Where length \overline{BC} denotes the distance between the centre line of a spherical particle and the intersecting point of a DNI ray skimming the particle into the glass, and \overline{ED} is the length between the

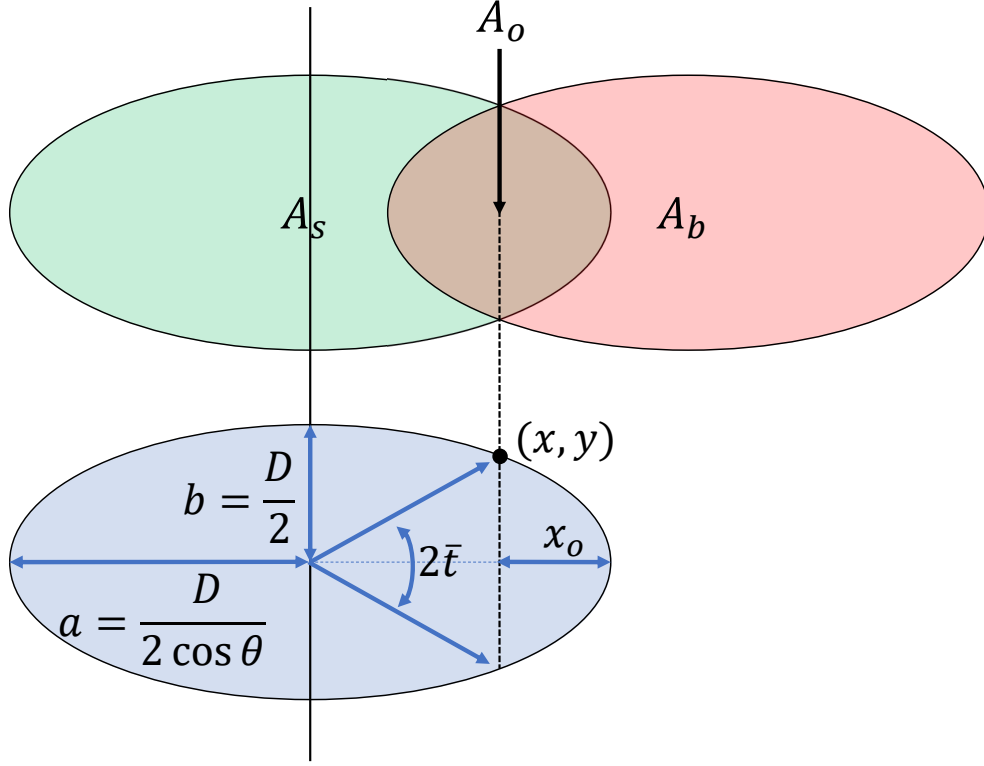


Figure A.21: Schematic of particle overlapping, shading and blocking areas

intersecting DNI point as projected onto the reflector vertically below and the final position of the ray before reflection. Overlapping will therefore only occur when $\overline{BC} > \overline{ED}$.

As DNI passes through the glass with thickness, t_g it will be refracted at a new angle. This ψ is calculated using Snell's law assuming a fixed refractive index for air and glass ($n_{air} = 1$ and $n_{glass} = 1.517$), \overline{ED} can be calculated using the refractive angle and thus the overlapping length is solved using Eq. A.3.

$$x_o = \overline{BC} - \overline{ED} \quad (\text{A.3a})$$

$$= \frac{D}{2} \tan\left(\frac{\beta}{2}\right) - t_g \tan(\psi) \quad (\text{A.3b})$$

$$= \frac{D}{2} \tan\left(\frac{90 - \theta}{2}\right) - t_g \tan\left(\sin^{-1}\left(\frac{n_{air}}{n_{glass}} \cdot \sin \theta\right)\right) \quad (\text{A.3c})$$

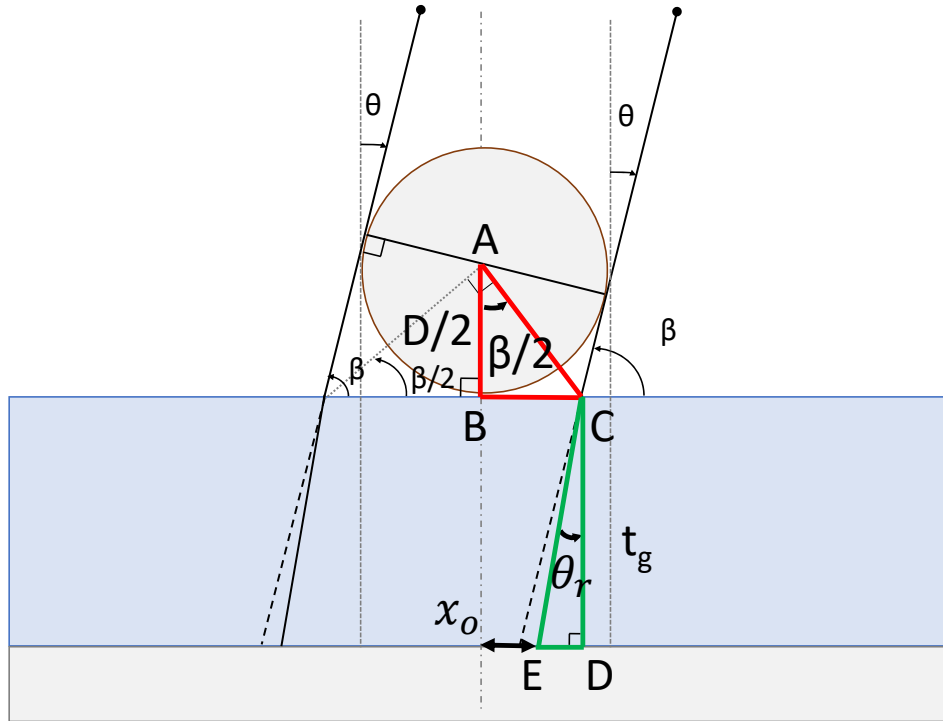


Figure A.22: Geometry diagram of shaded area boundary positions relative to a particle

References

- [1] IRENA, Renewable Capacity Statistics 2020, Technical Report, International Renewable Energy Agency, Abu Dhabi, 2020. URL: https://irena.org/-/media/Files/IRENA/Agency/Publication/2020/Mar/IRENA_RE_Capacity_Statistics_2020.pdf.
- [2] A. Bahadori, C. Nwaoha, A review on solar energy utilisation in Australia, Renewable and Sustainable Energy Reviews 18 (2013) 1–5. doi:10.1016/j.rser.2012.10.003.
- [3] D. Feldman, R. Margolis, P. Denholm, J. Stekli, Exploring the Potential Competitiveness of Utility-Scale Photovoltaics plus Batteries with Concentrating Solar Power, 2015 – 2030, Technical Report, NREL, Denver, CO, 2016. doi:10.2172/1321487.

- [4] G. Picotti, P. Borghesani, M. E. Cholette, G. Manzolini, Soiling of solar collectors – Modelling approaches for airborne dust and its interactions with surfaces, *Renewable and Sustainable Energy Reviews* 81 (2018) 2343–2357. URL: <http://dx.doi.org/10.1016/j.rser.2017.06.043>. doi:10.1016/j.rser.2017.06.043.
- [5] G. J. Kolb, C. K. Ho, T. R. Mancini, J. A. Gary, Power tower technology roadmap and cost reduction plan, Technical Report, Sandia Labs, Albuquerque, NM, and Livermore, CA (United States), 2011. doi:10.2172/1011644.
- [6] R. S. Berg, Heliostat dust buildup and cleaning studies, Technical Report SAND-78-0432C, Sandia Labs, Albuquerque, NM (United States), 1978. URL: <http://www.osti.gov/servlets/purl/6867834/>. doi:10.2172/6867834.
- [7] E. Roth, R. Pettit, The effect of soiling on solar mirrors and techniques used to maintain high reflectivity, Technical Report, Sandia Labs, Albuquerque, NM, and Livermore, CA (United States), 1980. doi:10.2172/5249717.
- [8] A. Heimsath, P. Nitz, The effect of soiling on the reflectance of solar reflector materials - Model for prediction of incidence angle dependent reflectance and attenuation due to dust deposition, *Solar Energy Materials and Solar Cells* 195 (2019) 258–268. doi:10.1016/j.solmat.2019.03.015.
- [9] G. Picotti, R. Simonetti, T. Schmidt, M. E. Cholette, A. Heimsath, S. J. Ernst, G. Manzolini, Evaluation of reflectance measurement techniques for artificially soiled solar reflectors: Experimental campaign and model assessment, *Solar Energy Materials and Solar Cells* 231 (2021) 111321. doi:10.1016/j.solmat.2021.111321.
- [10] G. Zhu, C. Augustine, R. Mitchell, M. Muller, P. Kurup, A. Zolan, S. Yellapantula, R. Brost, K. Armijo, J. Sment, R. Schaller, M. Gordon, M. Collins, J. Coventry, J. Pye, M. Cholette, G. Picotti, M. Arjomandi, M. Emes, D. Potter, M. Rae, G. Zhu, C. Augustine, R. Mitchell, M. Muller, P. Kurup, A. Zolan, S. Yellapantula, R. Brost, K. Armijo, J. Sment, R. Schaller, M. Gordon, M. Collins, J. Coventry, J. Pye, M. Cholette, G. Picotti, M. Arjomandi, M. Emes, D. Potter, M. Rae,

Roadmap to Advance Heliostat Technologies for Concentrating Solar-Thermal Power, Technical Report NREL/TP-5700-83041, NREL, 2022. URL: <https://www.nrel.gov/docs/fy22osti/83041.pdf>.

- [11] A. A. Hachicha, I. Al-Sawafta, D. Ben Hamadou, Numerical and experimental investigations of dust effect on CSP performance under United Arab Emirates weather conditions, *Renewable Energy* 143 (2019) 263–276. doi:10.1016/j.renene.2019.04.144.
- [12] A. Azouzoute, A. A. Merrouni, M. Garoum, E. G. Bennouna, Soiling loss of solar glass and mirror samples in the region with arid climate, *Energy Reports* 6 (2020) 693–698. doi:10.1016/j.egy.2019.09.051.
- [13] R. Conceição, A. Martínez Hernández, M. Romero, J. González-Aguilar, Experimental soiling assessment, characterization and modelling of a highly-compact heliostat field in an urban environment, *Solar Energy* 262 (2023) 111812. doi:10.1016/j.solener.2023.111812.
- [14] S. Bouaddi, A. Ihlal, A. Fernández-García, Soiled CSP solar reflectors modeling using dynamic linear models, *Solar Energy* 122 (2015) 847–863. doi:10.1016/j.solener.2015.09.044.
- [15] R. Conceição, H. G. Silva, M. Collares-Pereira, CSP mirror soiling characterization and modeling, *Solar Energy Materials and Solar Cells* 185 (2018) 233–239. doi:10.1016/j.solmat.2018.05.035.
- [16] M. Dehghan, S. Rashidi, A. Waqas, Modeling of soiling losses in solar energy systems, *Sustainable Energy Technologies and Assessments* 53 (2022) 102435. doi:10.1016/j.seta.2022.102435.
- [17] G. Picotti, P. Borghesani, G. Manzolini, M. Cholette, R. Wang, Development and experimental validation of a physical model for the soiling of mirrors for CSP industry applications, *Solar Energy* 173 (2018) 1287–1305. doi:10.1016/j.solener.2018.08.066.
- [18] M. Coello, L. Boyle, Simple Model for Predicting Time Series Soiling of Photovoltaic Panels, *IEEE Journal of Photovoltaics* 9 (2019) 1382–1387. doi:10.1109/JPHOTOV.2019.2919628.
- [19] S. Sengupta, S. Sengupta, H. Saha, Comprehensive Modeling of Dust Accumulation on PV Modules Through Dry Deposition Processes, *IEEE*

Journal of Photovoltaics 10 (2020) 1–10. doi:10.1109/jphotov.2020.2992352.

- [20] L. El Boujdaini, A. Mezrhab, M. Amine Moussaoui, J. Antonio Carballo Lopez, F. Wolfertstetter, The effect of soiling on the performance of solar mirror materials: Experimentation and modeling, *Sustainable Energy Technologies and Assessments* 53 (2022) 102741. doi:10.1016/j.seta.2022.102741.
- [21] F. Wolfertstetter, K. Pottler, N. Geuder, R. Affolter, A. A. Merrouni, A. Mezrhab, R. Pitz-Paal, Monitoring of mirror and sensor soiling with TraCS for improved quality of ground based irradiance measurements, *Energy Procedia* 49 (2014) 2422–2432. doi:10.1016/j.egypro.2014.03.257.
- [22] J. Ballestrín, J. Polo, N. Martín-Chivelet, J. Barbero, E. Carra, J. Alonso-Montesinos, A. Marzo, Soiling forecasting of solar plants: A combined heuristic approach and autoregressive model, *Energy* 239 (2022) 122442. doi:10.1016/j.energy.2021.122442.
- [23] G. Picotti, L. Moretti, M. E. Cholette, M. Binotti, R. Simonetti, E. Martelli, T. A. Steinberg, G. Manzolini, Optimization of cleaning strategies for heliostat fields in solar tower plants, *Solar Energy* 204 (2020) 501–514. doi:10.1016/j.solener.2020.04.032.
- [24] J. G. Wales, A. J. Zolan, A. M. Newman, M. J. Wagner, A. M. Newmans, M. J. Wagner, Optimizing Vehicle Fleet and Assignment for Concentrating Solar Power Plant Heliostat Washing, *IISE Transactions* 54 (2021) 550–562. doi:10.1080/24725854.2021.1966858.
- [25] F. Wolfertstetter, S. Wilbert, J. Dersch, S. Dieckmann, R. Pitz-Paal, A. Ghennioui, Integration of soiling-rate measurements and cleaning strategies in yield analysis of parabolic trough plants, *Journal of Solar Energy Engineering, Transactions of the ASME* 140 (2018) 4–8. doi:10.1115/1.4039631.
- [26] H. Truong Ba, M. E. Cholette, R. Wang, P. Borghesani, L. Ma, T. A. Steinberg, Optimal condition-based cleaning of solar power collectors, *Solar Energy* 157 (2017) 762–777. doi:10.1016/j.solener.2017.08.076.

- [27] H. Truong-Ba, M. E. Cholette, G. Picotti, T. A. Steinberg, G. Manzolini, Sectorial reflectance-based cleaning policy of heliostats for Solar Tower power plants, *Renewable Energy* 166 (2020) 176–189. doi:10.1016/j.renene.2020.11.129.
- [28] F. Sutter, M. Montecchi, H. von Dahlen, A. Fernández-García, M. Röger, The effect of incidence angle on the reflectance of solar mirrors, *Solar Energy Materials and Solar Cells* 176 (2018) 119–133. doi:10.1016/j.solmat.2017.11.029.
- [29] S. Karasu, A. Altan, Z. Sarac, R. Hacıoglu, Prediction of Solar Radiation Based on Machine, *The journal of cognitive systems* 2 (2017) 16–20. doi:10.1109/ICCONS.2018.8663110.
- [30] L. Zhang, J. Lin, R. Qiu, X. Hu, H. Zhang, Q. Chen, H. Tan, D. Lin, J. Wang, Trend analysis and forecast of PM2.5 in Fuzhou, China using the ARIMA model, *Ecological Indicators* 95 (2018) 702–710. doi:10.1016/j.ecolind.2018.08.032.
- [31] A. Altan, S. Karasu, E. Zio, A new hybrid model for wind speed forecasting combining long short-term memory neural network, decomposition methods and grey wolf optimizer, *Applied Soft Computing* 100 (2021) 106996. doi:10.1016/j.asoc.2020.106996.
- [32] R. Cleveland, W. Cleveland, M. JE, I. Terpenning, STL: A seasonal-trend decomposition, *Journal of Official Statistics* 6 (1990) 3–73. doi:10.1007/978-1-4613-4499-5{_}24.
- [33] G. J. McRae, W. R. Goodin, J. H. Seinfeld, Development of a second-generation mathematical model for Urban air pollution-I. Model formulation, *Atmospheric Environment* (1967) 16 (1982) 679–696. doi:10.1016/0004-6981(82)90386-9.
- [34] M. J. Wagner, T. Wendelin, SolarPILOT: A power tower solar field layout and characterization tool, *Solar Energy* 171 (2018) 185–196. doi:10.1016/j.solener.2018.06.063.
- [35] J. J. Michalsky, The Astronomical Almanac’s algorithm for approximate solar position (1950-2050), *Solar Energy* 40 (1988) 227–235. doi:10.1016/0038-092X(88)90045-X.

- [36] M. Guo, F. Sun, Z. Wang, J. Zhang, Properties of a general azimuth-elevation tracking angle formula for a heliostat with a mirror-pivot offset and other angular errors, *Solar Energy* 96 (2013) 159–167. doi:10.1016/j.solener.2013.06.031.
- [37] R. D. Grisso, M. F. Kocher, D. H. Vaughan, Predicting tractor fuel consumption, *Applied Engineering in Agriculture* 20 (2004) 553–561. doi:10.13031/2013.13732.
- [38] Queensland Government, Electricity supply options for the North West Minerals Province - CRIS, Technical Report December, Queensland Government, 2021. URL: https://www.epw.qld.gov.au/___data/assets/pdf_file/0023/19715/north-west-electricity-province-cris.pdf.
- [39] Z. Xuzhong, X. Neng, M. Xiaoling, C. Kangli, H. Long, H. Yuchao, X. Gangqiang, L. Xiaobo, Cleaning Vehicle, Technical Report, SUPCON SOLAR, 2020. URL: <https://www.solarpaces.org/wp-content/uploads/1-1-page-description-of-the-innovative-idea-and-its-impact-and-the-role-of-t.pdf>.
- [40] M. Hardt, D. Martínez, A. González, C. Garrido, S. Aladren, J. R. Villa, J. Saenz, HECTOR – heliostat cleaning team-oriented robot, *SolarPaces Conference* (2011) 20–23.
- [41] Vast Solar, Presentation at ASTRI Annual Workshop Public Symposium, 2016. URL: https://www.astri.org.au/wp-content/uploads/2016/04/ASTRI-20160502-1450-James_Fisher-Vast_Solar.pdf.

Nomenclature

Latin

A^{block} area lost due to blocking

A^{loss} area lost due to soiling

A^{norm} area loss at normal incidence

A^{overlap} overlapped area of shading and blocking regions

A^{shade} area lost due to shading
 A^{mirror} heliostat mirror area
 A^{total} total heliostat area
 D particle diameter
 F annual field cleanings per heliostat
 M number of trucks
 N cumulative particle number distribution
 P price of electricity
 Q^{array} receiver array energy output
 Q^{field} field-array reflected energy at receiver
 Q^{loss} constant receiver thermal energy loss
 Q^{max} maximum allowable receiver energy
 Q^{pb} power block thermal energy input
 Q^{rec} total receiver energy output
 Q^{tes} thermal energy storage output
 R sectors cleaned per crew
 T ambient temperature
 U uptime ratio
 \mathcal{D} cleaning action time
 C^{cl} cleaning cost
 C^{deg} degradation cost
 C^{maint} truck maintenance cost
 $C^{\text{o\&m}}$ operation and maintenance costs

C^{op} operation cost
 C^{salary} operator salary
 C^{truck} truck cost
 $C^{\text{w\&f}}$ water and fuel costs
 ζ cleanliness
 a area loss due to a particle
 b asset depreciation time
 g geometry factor
 h_r/z_o surface roughness ratio
 n particle number size distribution deposition rate
 s^{max} maximum storage charge
 s thermal storage charge
 t_g glass thickness
 v wind speed
 w^{clean} work produced with clean field
 w^{dayC} work produced with clean field and daytime cleaning
 w^{rated} rated power block work
 w^{soil} work produced with soiled field
 w work produced
 x_o overlap length

Greek

Δk days between successive field cleanings

Δt_d sampling periods in a day

Δt time between epochs

\bar{t} eccentric anomaly

η^{opt} optical efficiency

η_{cl} cleaning efficiency

η_{pb} power block efficiency

$\hat{\rho}$ reflectance prediction

ϕ tilt angle

ψ refracted angle

ρ measured reflectance

θ incidence angle

Subscripts

J total number of heliostat sectors

K total number of time epochs

L number of receivers

ℓ target receiver index

j heliostat sector index

k time index

Acronyms

DNI direct normal irradiance

SZA solar zenith angle

TCC total cleaning cost

ANN artificial neural network

ARMA autoregressive-moving-average model

CARF Central Analytical Research Facility

CSP concentrated solar power

DSM dry-deposition soiling model

FFTBCS fixed-frequency-time-based cleaning schedule

MSE mean squared error

NWQHPP North-West Queensland Hybrid Power Plant

O&M operation and maintenance

PV photovoltaic

QUT Queensland University of Technology

TES thermal energy storage

TraCs Tracking Cleanliness Sensor

TSP total suspended particles

XRD Xray diffraction